LA-14421
Approved for public release;
distribution is unlimited.

The MGGB Equation-of-State for Multifield Applications: A Numerical Recipe for Analytic Expression of Sesame EOS Data

Los Alamos
NATIONAL LABORATORY
EST. 1943

Edited by Hector Hinojosa, Group IRM-CAS.

Los Alamos National Laboratory, an affirmative action/ equal opportunity employer, is operated by Los Alamos National Security, LLC, for the National Nuclear Security Administration of the U.S. Department of Energy under contract DE-AC52-06NA25396.

LA-14421
Issued: September 2010

The MGGB Equation-of-State for Multifield Applications: A Numerical Recipe for Analytic Expression of Sesame EOS Data

B. A. Kashiwa

Los Alamos
NATIONAL LABORATORY
EST. 1943

CONTENTS

This page is mostly blank.

The MGGB Equation–of–State for Multifield Applications:

A numerical recipe for analytic expression of Sesame EOS data

B. A. Kashiwa

Abstract A thermodynamically consistent and fully general equation–of–state (EOS) for multifield applications is described. EOS functions are derived from a Helmholtz free energy expressed as the sum of thermal (fluctuational) and collisional (condensed–phase) contributions; thus the free energy is of the Mie–Grüneisen[1] form. The phase–coexistence region is defined using a parameterized saturation curve by extending the form introduced by Guggenheim,[2] which scales the curve relative to conditions at the critical point. We use the zero–temperature condensed–phase contribution developed by Barnes,[3] which extends the Thomas–Fermi–Dirac equation to zero pressure. Thus, the functional form of the EOS could be called MGGB (for Mie–Grüneisen–Guggenheim–Barnes). Substance–specific parameters are obtained by fitting the low–density energy to data from the Sesame[4] library; fitting the zero–temperature pressure to the Sesame cold curve; and fitting the saturation curve and latent heat to laboratory data,[5] if available. When suitable coexistence data, or Sesame data, are not available, then we apply the Principle of Corresponding States.[2] Thus MGGB can be thought of as a numerical recipe for rendering the tabular Sesame EOS data in an analytic form that includes a proper coexistence region, and which permits the accurate calculation of derivatives associated with compressibility, expansivity, Joule coefficient, and specific heat, all of which are required for multifield applications.

I. INTRODUCTION

The goal of this work is to devise a reliable means of expressing equation–of–state (EOS) data in a form suitable for general multifield problems. By "general" we mean permitting *all possible* values of density and temperature. By "multifield" we mean the *averaged* continuum dynamics of a set of substances, each member of the set having a well–defined EOS. Given this collection of substances, the averaged multifield EOS evaluation of specific interest here can be stated as follows. Let $N_{\rm f}$ signify the size of the set. Using the integer index subscript r, unique to a given member of the set, let $\tilde{p}_{\rm r}\left[v_{\rm r}, T_{\rm r}\right]$ signify its pressure and $\tilde{e}_{\rm r}\left[v_{\rm r}, T_{\rm r}\right]$ signify its specific internal energy. In classical terms $\tilde{p}_{\rm r}$ and $\tilde{e}_{\rm r}$ are *thermal* and *caloric* equations of state, both functions of the specific volume v and temperature T. Further, let V be a volume containing a distribution of masses $M_{\rm r}$, each of which has a given specific internal energy $e_{\rm r}$. The multifield EOS of interest here is

$$V - \sum_{\rm r=1}^{N_{\rm f}} M_{\rm r} v_{\rm r} = 0 \tag{1}$$

$$p - \tilde{p}_{\rm r}\left[v_{\rm r}, T_{\rm r}\right] = 0 \quad {\rm r} = (1, 2, \ldots, N_{\rm f}) \tag{2}$$

$$e_{\rm r} - \tilde{e}_{\rm r}\left[v_{\rm r}, T_{\rm r}\right] = 0 \quad {\rm r} = (1, 2, \ldots, N_{\rm f}) \tag{3}$$

a system of $2N_{\rm f}+1$ equations in the $2N_{\rm f}+1$ unknowns $(p, v_{\rm r}, T_{\rm r})$. This is a semi–equilibrium approximation. It is assumed that the $N_{\rm f}$ substances at the same space–time point $[\mathbf{x}, t]$ will, *on average*, exhibit the same pressure, but they may not share the same temperature (or the same velocity). The *fully* equilibrium approximation, of course, assumes that all fields have achieved a state having single–valued pressure, temperature, and velocity.

Evaluation of the system (1–3) is a nonlinear root finding problem. In multifield numerical simulations this system is typically solved at a large number of discrete space–time points. The computational speed, robustness, accuracy, and validity of multifield dynamical simulations are all heavily dependent on the nature of the multifield EOS. Therefore, it is sensible to engage in a dedicated effort whose object is to formulate thermal and caloric EOS functions that are true to the physical data, numerically tractable, and thermodynamically consistent. This report is the result of one such effort. The means by which the objective is approached is in no way unique; the methods of expression used here are closely aligned with time–honored ones that have been found useful by a collection of prior investigators far too numerous to name. Very loosely, the methods employed here are analogous to those used for constructing the Sesame[4] tabular EOS database, with extensions that become clear in later sections.

Multifield theory is a continuum approach to problems in dynamics that involve several distinct materials, separated in space, interacting at material interfaces, and for which Local Thermodynamic Equilibrium is a good approximation. In this theory it is also assumed, from the outset, that a complete description of the dynamics for each material, taken in isolation (that is, without regard to other materials) is available. For example, in classical fluid dynamics problems a complete continuum description is provided by the conservation laws for mass, linear momentum and total energy, plus closure data. The closure data, which are material–specific, include complete equations of state, heat conduction data, and a material response function. One simple form of material response, is that of an isotropic viscous fluid, for which the stress is expressed using a single coefficient of viscosity and local–instantaneous gradients of the velocity. An equally simple material response is that of an elastic isotropic solid material for which the rate of change of the stress is given by two elastic constants and the strain rate (a tensor–valued object formed, typically, by local–instantaneous velocity gradients). In general, the material response may be elasto–plastic, viscoelastic, thixotropic, or other strange nonideal responses that can be the cause of interesting effects. For any material response the multifield EOS must be evaluated: the effects of this evaluation will ultimately feed back into, and influence, the material response.

The basis for multifield theory consists of the classical continuum conservation laws subjected to an averaging procedure that permits a finite probability for *any one* of the $N_{\rm f}$ possible materials to occupy a space–time point. Ensemble averaging is convenient for this purpose, and the result is a system of unclosed conservation laws for the averaged collective dynamics of the $N_{\rm f}$ material set. These are continuum field equations for which the entirety of multifield theory is occupied with the problem of devising closure relations for interactions among the fields. Multifield closures are needed for the turbulent stress; turbulent heat flux; exchanges of mass, linear momentum and total energy among fields; averaged equations of state; and averaged material response.[6,7] This report considers only one of these closure problems, namely, the EOS closure.

One very common EOS closure assumption is to suppose that the statistical expectation for a particular substance residing at a space–time point is equal to its averaged volume fraction $\theta_{\rm r}\left[\mathbf{x},t\right]$, whereby

$$\theta_{\rm r} = M_{\rm r} v_{\rm r}/V = \rho_{\rm r} v_{\rm r} \tag{4}$$

This may be the most common assumption used in multifield theory, and it is the one used here; having made it the multifield EOS expressed in (1–3) follows; the problem is that of finding the value of pressure p, such that all materials will fill the volume V, given a specified collection of masses and internal energies.

Because the system (1–3) may involve materials at any point of $[v, T]$ space (such as a gas and a solid), the only way to guarantee existence of a solution is to permit phase–coexistence in the EOS for all materials. In this way $\tilde{p}_\mathrm{r} \geq 0$, for all r, and a solution will always exist.

Multifield applications are typically concerned with the forward–time integration of conservation equations using discrete numerical approximations. One very common approximation uses a first–order Taylor series expansion in time, in order to advance the thermodynamic state during the integration. Let the overdot signify the Lagrangian (material–frame) derivative. Using (4) and standard symbols for specific heat c_v; isothermal compressibility κ; and constant pressure expansivity β; the Taylor expansions for energy and volume are

$$\rho_\mathrm{r}\dot{e}_\mathrm{r} = \rho_\mathrm{r}\left(c_{v\mathrm{r}}\dot{T}_\mathrm{r} + e_{,v\mathrm{r}}\dot{v}_\mathrm{r}\right) = \text{work, chemistry, heat transport, heat exchange} \quad (5)$$

$$\rho_\mathrm{r}\dot{v}_\mathrm{r} = \theta_\mathrm{r}\left(-\kappa_\mathrm{r}\dot{p} + \beta_\mathrm{r}\dot{T}_\mathrm{r}\right) = \text{thermal expansion, volume exchange, dilation} \quad (6)$$

where $e_{,v}$ is the derivative of energy with respect to specific volume. Hence, derivatives of the EOS become coupling coefficients for changes in energy and specific volume. Accurate values of these derivatives are generally unavailable when the EOS is furnished in tabular form, which is a significant motivating factor behind this report.

The right side of (5) contains the physics of energy evolution, which is common knowledge. The right side of (6) is less commonly known — it is determined by taking the time derivative of (1), for which the mass conservation equation is needed. That is

$$\frac{\partial \rho_\mathrm{r}}{\partial t} + \boldsymbol{\nabla} \cdot \rho_\mathrm{r}\mathbf{u}_\mathrm{r} = \Gamma_\mathrm{r} \quad (7)$$

where ρ_r is the mass of field–r material, per unit of volume, and Γ_r is the source due to conversion to/from other fields. The mass conservation equation, summed on all fields, can be combined with the volume rate to obtain

$$\boldsymbol{\nabla} \cdot \mathbf{u} - \sum \rho_\mathrm{s}\dot{v}_\mathrm{s} = \sum v_\mathrm{s}\Gamma_\mathrm{s} \quad (8)$$

where the velocity $\mathbf{u} = \sum \theta_\mathrm{s}\mathbf{u}_\mathrm{s}$ is the total volume flux. The volume sum in (8) is set to the field–sum of (6) and solved for $\dot{p}$. That is

$$\dot{p} = \frac{\sum \theta_\mathrm{s}\beta_\mathrm{s}\dot{T}_\mathrm{s} + \sum v_\mathrm{s}\Gamma_\mathrm{s} - \boldsymbol{\nabla} \cdot \mathbf{u}}{\sum \theta_\mathrm{s}\kappa_\mathrm{s}} \quad (9)$$

This in turn is placed in (6) to determine the physical evolution of r–field specific volume, subject to satisfying the time–derivative of the EOS:

$$\rho_{\rm r}\dot{v}_{\rm r} = \left(\theta_{\rm r}\beta_{\rm r}\dot{T}_{\rm r} - f^{\theta}_{\rm r}\sum\theta_{\rm s}\beta_{\rm s}\dot{T}_{\rm s}\right) - f^{\theta}_{\rm r}\sum v_{\rm s}\Gamma_{\rm s} + f^{\theta}_{\rm r}\boldsymbol{\nabla}\cdot\mathbf{u} \tag{10}$$

where

$$f^{\theta}_{\rm r} = \frac{\theta_{\rm r}\kappa_{\rm r}}{\sum\theta_{\rm s}\kappa_{\rm s}} \tag{11}$$

is clearly a fraction that lies between zero and one. This fraction shows that the total volume dilation is distributed among materials according to their relative compressibility. The conservative form of (10) is found by adding $v_{\rm r}$ times the r–mass equation. It is

$$(\rho_{\rm r}v_{\rm r})^{\cdot} = \left(\theta_{\rm r}\beta_{\rm r}\dot{T}_{\rm r} - f^{\theta}_{\rm r}\sum\theta_{\rm s}\beta_{\rm s}\dot{T}_{\rm s}\right) + \left(v_{\rm r}\Gamma_{\rm r} - f^{\theta}_{\rm r}\sum v_{\rm s}\Gamma_{\rm s}\right) + f^{\theta}_{\rm r}\boldsymbol{\nabla}\cdot\mathbf{u} \tag{12}$$

By inspection $\sum(\rho_{\rm r}v_{\rm r})^{\cdot} = \boldsymbol{\nabla}\cdot\mathbf{u}$; which is a well–known kinematic condition on the total volume rate.

Historically the EOS for materials that can sustain a certain amount of tensile stress in the solid phase have been generated; this means that regions of negative pressure were included in such a way that the EOS would furnish the isotropic part of the material stress. The deviatoric part was furnished by a relationship separate from the EOS evaluation. In the present approach to problems with a solid–phase material strength we instead provide *full* material stress by means of integrating in time a stress history equation.[6,7] This method permits a completely unrestricted material stress to develop; meaning that the stress response to straining motions may be isotropic or anisotropic, and the stress can exhibit an arbitrarily large state of tension or compression. Insofar as the stress is concerned in this method, the role of the EOS is to provide an accurate determination of the present $[v, T]$ state (which may have a profound effect on the evolution of the stress).

To reiterate, the central thrust of this report is the analytic expression of EOS data that has been developed and reported elsewhere, and in a form needed for multifield applications. Hence the physical, theoretical, and experimental details that underlie the EOS data itself are not described here; this information is readily available in the literature cited in the text. Any connection with the fundamentals of statistical physics is mentioned only very briefly in areas where it may be helpful to provide the genesis of certain functional forms used here.

The report is organized as follows. In §II we describe the EOS parameterization beginning with an extended form of the Mie–Grüneisen[1] Helmholtz free energy similar in spirit to the one used by Sewell & Menikoff;[8] the coexistence region is defined by tailoring the universal one originally given by Gueggenheim;[2] and with the solid–phase contribution in the form developed by Barnes;[3] in §III we illustrate the means by which substance–specific parameters are found by fitting to Sesame[4] data, and we compare the results to the original Sesame data for dry air[9], water[10], methane[11], aluminum[12], copper[13], and tungsten[14]; §IV describes a robust numerical procedure for solving the nonlinear problem posed by (1–3); and §V is a discussion of areas in which some follow–on work may prove valuable. Appendices are used liberally to harbor summaries, standard knowledge, and tricks that are handy, typically elementary, and easy to forget.

II. THE MGGB EOS IN FUNCTIONAL FORM

Viewed from a sufficiently high level, the procedure described here will appear to be very similar to the one used for many of the EOS data tables in the Sesame[4] library. This procedure begins by defining a Helmholtz free energy in a general parametric functional form. This form is supposed to reflect the equilibrium statistics of a large collection of "particles" (atoms or molecules) over the range of density–temperature space considered. Parameters appropriate for any given substance are determined from a large variety theoretical and experimental means. Given the parameters and the Helmholtz free energy, the caloric and thermal EOS are completely determined by differentiation. If we let $F[v,T]$ signify the Helmholtz free energy for any substance as a function of specific volume v and temperature T, then by definition the pressure $p[v,T]$, entropy $s[v,T]$, and specific internal energy $e[v,T]$ are

$$p[v,T] = -\frac{\partial F}{\partial v}$$

$$s[v,T] = -\frac{\partial F}{\partial T}$$

$$e[v,T] = F + Ts$$

In general F is expressed in terms of a sum of parts that represent the contributions of various physical effects. Here we consider F to be the sum of two parts: one for the contribution due to thermal fluctuations, called the thermal part, and signified by the subscript T; and another for the contribution due to collisional forces, called the condensed–phase part, and signified by the subscript ϕ. This two–part F was used almost exclusively in the early Sesame[4]

database. (A more comprehensive additive approach is described, for example, by Chisolm.[15])

It has long been recognized that EOS functions of the form used here are capable of exhibiting so–called "critical phenomena," said to arise when the interparticle force becomes sufficiently attractive.[16] For multifield problems the critical phenomenon of most interest is phase–coexistence. When conditions are such that a gas and its condensed phase can coexist in equilibrium (which is said to be metastable) the region of v–T space within which such states reside can be derived from the EOS by means of a so–called "Maxwell's construction." This is a process by which a region of $F[v,T]$ space below the critical temperature is replaced by a linear variation in v, and whose limits are given by conditions on $F[v,T]$ itself.[16] Having performed this construction, a well–defined coexistence region has been found; in this region the pressure is positive (or negligibly small) and constant on isotherms.

Most but not all of the Sesame data exclude the coexistence region. Tables for the metals such as copper, aluminum, and tungsten do not; one table for water does; and for methane there are tables both with and without a region of coexistence. Here we use, in effect, a parameterized form of Maxwell's construction that is rooted in the work summarized by Guggenheim[2] and called "The Principle of Corresponding States." In this Guggenheim showed that the saturation curve and latent heat, defining the coexistence region, are readily parameterized in terms of the critical temperature. We make use of this parameterization to carry the results of Maxwell's construction, and show that the result is sensible in view of both Sesame and experimental data.

For simplicity we ignore the distinction between the liquid and solid phase, so that the volume discontinuity connected with melting/freezing phenomena is not explicitly included; thus a triple point does not appear. Nevertheless the energetics of condensation (or sublimation) are fully contained in the EOS. Hence our coexistence region spans the transition from pure gas to pure "condensed–phase;" we use the subscript g for gas and the subscript n for the condensed–phase ("not–gas"), so that $\rho_g[T] = 1/v_g[T]$ is the density of saturated gas and $\rho_n[T] = 1/v_n[T]$ is the density of saturated condensed–phase. As an aid to describing how the coexistence region is determined, we divide the $[v,T]$ domain into a pentad of regions according to Fig. 1, where dashed lines signify the saturation curve. In this figure Region I is entirely gas–phase, and contains all temperatures greater than the critical temperature T_c and all densities to the expansion side of the critical density; Region II is subcritical gas–phase with all densities expanded relative to the saturation curve; Region III is the coexistence region; Region IV is the subcritical condensed–phase, and Region V is the supercritical condensed–phase.

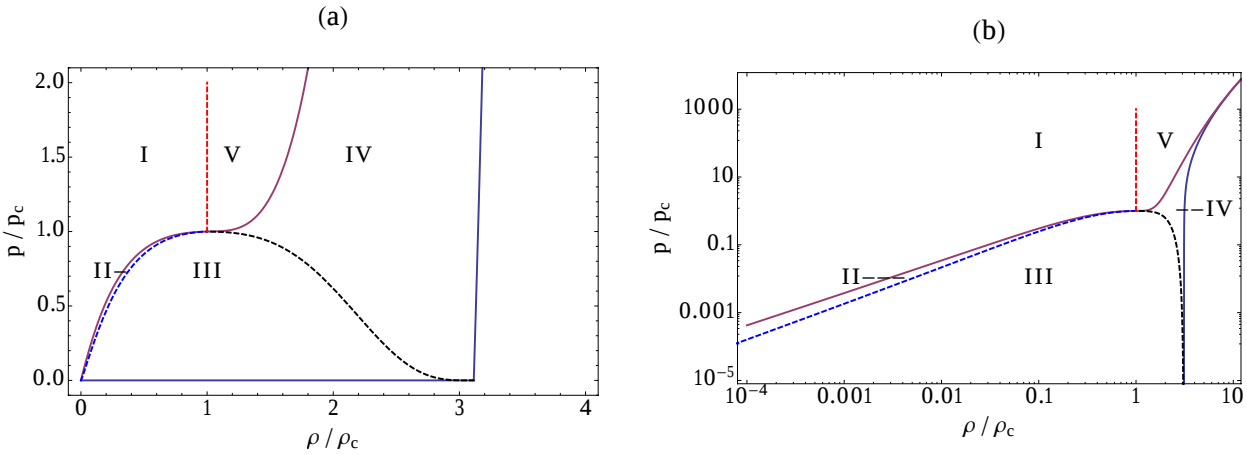

Figure 1. Definition of the region pentad. (a) Linear scale; (b) Log-Log scale; in both plots the dashed line identifies the saturation curve, which has a branch–cut extending from the critical temperature to infinity. Red line is the critical isotherm; blue is the cold curve. Region I is supercritical and to the expanded side of the saturation curve; Region II is subcritical and to the expanded side of the saturation curve; Region III is the coexistence region; Region IV is the subcritical condensed–phase region; and Region V is supercritical condensed–phase.

A. Extended Mie–Grüneisen: The Helmholtz Free Energy

We extend the Helmholtz function used by Sewell & Menikoff,[8] by adding the cohesive energy $e_\circ$ corresponding to $v = v_\circ$ and $T = 0$:

$$F\left[v,T\right] = -v_\circ \int_1^{v/v_n} p_\phi\left[\eta\right]\ d\xi - \Theta \int_0^{T/\Theta} C\left[\tau\right]\left(\frac{T}{\Theta} - \tau\right)\ \frac{d\tau}{\tau} + e_\circ \tag{13}$$

where the dummy variable $\eta = 1/\xi$. We further extend by permitting the scaling temperature $\Theta\left[v,T\right]$ to be a function of both volume and temperature; and we permit the upper limit of the condensed–phase contribution to be a function of temperature, by way of $v_n\left[T\right]$, in order to provide a smooth transition into the compressed condensed–phase region, details of which are given in section II C. In (13) the first integral is the collisional contribution (expressed in terms of the compression of the condensed–phase, so it is understood that the upper limit is $\min\left[1, v/v_n\right]$ because p_ϕ is nonnegative). The second integral is the fluctuational (thermal) contribution. By differentiation we have

$$p\left[v,T\right] = -\frac{\partial e_\phi}{\partial v} - \frac{e_{_T}}{v}\frac{\partial \log\Theta}{\partial \log v} \tag{14}$$

$$s\left[v,T\right] = -\frac{\partial e_\phi}{\partial T} - \frac{e_{_T}}{T}\frac{\partial \log\Theta}{\partial \log T} + s_{_T} \tag{15}$$

$$e\left[v,T\right] = \left(e_\phi - T\frac{\partial e_\phi}{\partial T}\right) + e_{_T}\left(1 - \frac{\partial \log\Theta}{\partial \log T}\right) + e_\circ \tag{16}$$

where we signify the integrals by

$$e_\phi\,[v,T] = -v_\circ \int_1^{v/v_n} p_\phi\,[\eta]\;\; d\xi \tag{17}$$

$$e_{_T}\,[v,T] = \Theta \int_0^{T/\Theta} C\,[\tau]\;\; d\tau \tag{18}$$

$$s_{_T}\,[v,T] = \int_0^{T/\Theta} \frac{C\,[\tau]}{\tau}\; d\tau \tag{19}$$

Equation (14) may be recognized as identical to that which was displayed by Grüneisen[1] where we use $(v, e_\phi, e_{_T})$ in place of (V, Φ, E). For this reason we refer to (13) as having the Mie–Grüneisen functional form. Following Sewell & Menikoff [8] we define

$$\Gamma_V\,[v,T] \equiv -\frac{\partial \log \Theta}{\partial \log v} \tag{20}$$

It is also convenient to define

$$\Gamma_T\,[v,T] \equiv -\frac{\partial \log \Theta}{\partial \log T} \tag{21}$$

Here we use

$$C\,[\tau] = C_\circ\big(1 + c_1 H_\circ\,[\tau/\Theta_1, d_1]\big) \tag{22}$$

$$\Gamma_\circ\,[T] = c_2 + \left(\tfrac{2}{3} - c_2\right) H_\circ[T/\Theta_2, d_2] \tag{23}$$

$$b\,[T] = c_3 H_1[T/T_c, d_3] \tag{24}$$

where $C_\circ = 3R/\hat{M}$ a reference specific heat, per unit mass, in which R is the gas constant, and $\hat{M}$ is the substance weight (either atomic or mean molecular), per mole. Also $H_\circ[x,y]$ is an Heaviside function centered at x, and having width $y \log x$; accordingly it has the value $H_\circ[1,y] = 1/2$. This function is described in full detail in Appendix A, along with its normalized derivative $H_1[x,y]$ which looks like a Delta function with $H_1[1,y] = 1$. Differentiation of the integral functions is a straightforward matter using Leibnitz's rule, and is shown in Appendix B. The integral expressions are displayed in Appendix C.

We modify the Sewell–Menikoff expression for Γ_V such that

$$\Gamma_V\,[v,T] = \Gamma_\circ - b H_1[\eta_c, d_4] \tag{25}$$

in which

$$\eta_c\left[v\right] = \left(\alpha\frac{v}{v_\circ} + (1-\alpha)\frac{v}{v_c}\right)^{-1} \tag{26}$$

where α is another substance–dependent constant. By integration we have

$$\Theta\left[v,T\right] = \eta_c^{\Gamma_\circ}\mathrm{e}^{-bH_z} \tag{27}$$

where $H_z = (\sqrt{\pi}/2d_4)\mathrm{Erf}[d_4\log\eta_c]$; and by differentiation we have

$$\Gamma_T\left[v,T\right] = Tb'H_z - T\Gamma'_\circ\log\eta_c \tag{28}$$

where the prime signifies differentiation with respect to the single independent variable T.

To summarize what we have so far, (14–28) define parameterized equations of state. For any substance, these depend on the 15 parameters

$$\left(T_c, v_c, v_\circ, e_\circ, \hat{M}, \Theta_1, \Theta_2, c_1, c_2, c_3, d_1, d_2, d_3, d_4, \alpha\right)$$

In the next section we display the parameterization of the coexistence region, which adds four more parameters associated with defining the saturation curve and the latent heat. These four are signified by

$$(q, r, \rho_z, \sigma)$$

Then we complete the parameter inventory with three more substance–specific constants that define the condensed–phase pressure function $p_\phi[\eta]$, given in § II C, and signified by

$$(B_\circ, b_a, b_r)$$

which is the same nomenclature used by Barnes.[3] This brings the grand total of parameters to 22, which are determined in §III.

B. Extended Guggenheim: The Coexistence Region

To define the coexistence region we extend the functions given by Guggenheim[2] for the lines of saturated vapor and saturated liquid. Using $\tau = T/T_c \leq 1$ (which is not to be confused with the dummy variable used in the energy integrals), those functions are

$$\rho_g\left[\tau\right]/\rho_c = 1 + (3/4)\left(1-\tau\right) - (7/4)\left(1-\tau\right)^{1/3} \tag{29}$$

$$\rho_n\left[\tau\right]/\rho_c = 1 + (3/4)\left(1-\tau\right) + (7/4)\left(1-\tau\right)^{1/3} \tag{30}$$

$$\rho_c = (2/7)\,\rho_\circ \tag{31}$$

where, again, we use the subscript "g" for gas, and "n" for the condensed–phase, and where we use $(\rho_\circ = 1/v_\circ;\ \rho_c = 1/v_c)$, both constants. These functions are fits to a large collection of experimental data; they are considered to be applicable to any substance for which the Principle of Corresponding States applies, which is supposed to include any element, nonpolar molecule, or mixture thereof.

Here we extend the saturation functions in two essential ways: 1) for saturated gas a particular exponential form is selected in order to obtain a finite latent heat at zero temperature; and 2) the polynomial form for the saturated condensed–phase is modified in order to permit fitting to data for any substance, including polar molecules (like water). These extended functions are

$$\rho_g\left[\tau\right]/\rho_c = \exp\left[-\left(q/\tau\right)\left(1-\tau\right)^r\right] \tag{32}$$

$$\rho_n\left[\tau\right]/\rho_c = 1 + \left(\zeta - 1\right)\left(1-\tau\right)^{0.48} \tag{33}$$

$$\zeta = \left(\rho_z/\rho_c\right)\tau^{1.30} + \left(\rho_\circ/\rho_c\right)\left(1-\tau^{1.30}\right) \tag{34}$$

where we introduce three new variable parameters (q, r, ρ_z), and two fixed ones $(0.48, 1.30)$. The motive for these selections is given shortly. The extended functions are compared with (29–31) in Fig. 2. There we use $(q, r, \rho_z/\rho_\circ) = (4.50, 0.54, 1.00)$, which we regard as a "universal" parameter set because the functions fit the experimental data equally as well as do (29–31). By "universal" we simply mean that the functions define the saturation curve for any substance for which the Principle of Corresponding States applies. The practical utility of (32–34) is that they provide a means of fitting data for any substance, if that data were to exist, and a useful gauge for any other substance assumed to obey the Principle of Corresponding States.

The motive behind the variable factor ζ in (32–34) is to allow more flexibility in the process of fitting experimental data for the saturated condensed–phase side of the curve, particularly for substances having a polar molecule — which typically excludes them from obeying the Principle of Corresponding States. This added feature is used here mainly to accommodate water, because of its importance in many problems of interest. The quantitative effect of this factor is shown later when we display plots of the EOS in comparison to experimental data.

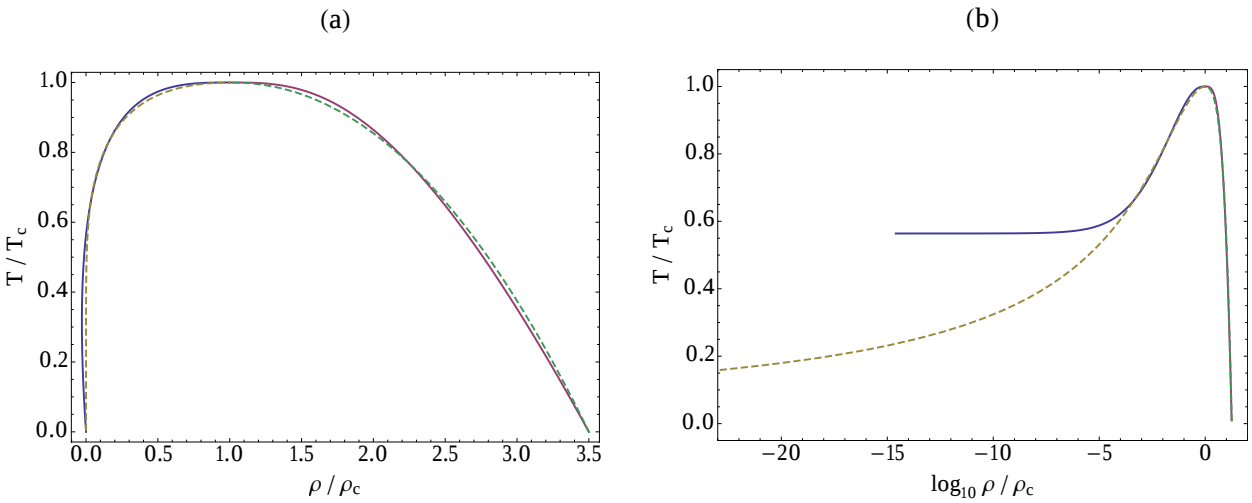

Figure 2. The Extended Guggenheim saturation curve. (a) Linear scale; (b) Log-Linear scale; in both plots solid lines correspond to (29–31); dashed lines correspond to (32–34).

The exponential form used in (32) for the density of saturated gas is suggested by the expression we use for the latent heat $\Delta h\,[T] = h_n - h_g < 0$ where $h = e + pv$ is the enthalpy. We find that a simple form involving one new variable parameter provides a good correlation to the latent heat data for all substances. Using σ for the latent heat parameter, this form is

$$\Delta h\,[T] = \sigma \Gamma_\circ C T \log\left[\rho_g/\rho_n\right] \tag{35}$$

where the functions $(\Gamma_\circ\,[T]\,, C\,[T])$ are given by (22–23). Using (32–34) we have

$$\Delta h_\circ = \lim_{T\to 0} \Delta h = -q\sigma c_2 C_\circ T_c \tag{36}$$

a substance–specific constant, which turns out to be very similar in magnitude to the cohesive energy $e_\circ$ for the selection of materials studied here. Indeed, if we were to set $e_\circ = -\Delta h_\circ$ then the value of energy at normal density and zero temperature would be $e\,[v_\circ, 0] = 0$. (Because the reference energy is arbitrary, it is tempting to use $e_\circ = -\Delta h_\circ$ simply for the sake of tidiness — but we refrain from doing so in order to facilitate comparison with the Sesame data, which furnish $e_\circ$ explicitly.)

Now let the subscript s signify conditions in Region III, and let $(v_g[T], v_n[T]) = (1/\rho_g[T], 1/\rho_n[T])$. With these symbols our Maxwell's construction is as follows. The saturation pressure is simply

$$p_s\,[T] = p\,[v_g, T] \tag{37}$$

which is constant on isotherms. The energy at any point in Region III is

$$e_s\,[v, T] = e\,[v_g, T] + \Delta h \left(\frac{v - v_g}{v_n - v_g}\right) - p_s\,(v - v_g) \tag{38}$$

which corresponds to replacing $F\left[v,T\right]$ with a linear function in v, as was suggested by Maxwell. Formally this requires matching the Gibbs free energy, $g = F + pv = h - Ts$, for saturated gas to that for saturated condensed–phase. At a specified value of $T < T_c$ there there will be one value of pressure p_s that satisfies

$$\begin{aligned} F\big[v_n,T\big] - F\big[v_g,T\big] + p_s\big(v_n - v_g\big) &= 0 \\ p\left[v_n,T\right] - p_s &= 0 \\ p\left[v_g,T\right] - p_s &= 0 \end{aligned} \tag{39}$$

where $\big(F\left[v,T\right],p\left[v,T\right]\big)$ are given by (13–14). The solution gives the latent heat

$$\Delta h = T\big(s\left[v_n,T\right] - s\left[v_g,T\right]\big) \tag{40}$$

where s is given by (15). Hence the saturation curve given by (32–34), and the latent heat given by (35), represent a parameterization of the root finding problem (39–40) posed by Maxwell for construction of the coexistence region.

C. Extended Barnes: The Condensed–Phase Contribution

For the condensed–phase contribution in (13) we utilize the Barnes[3] zero–temperature pressure function, which extends the so–called Thomas–Fermi–Dirac equation to a the proper limit $p_\phi\left[1\right] = 0$, using an experimentally measured bulk modulus $B_\circ$. This function is used in the construction of tables for many (if not most) of the materials in the Sesame[4] tabular EOS library. Barnes originally developed this in terms of the compression $\eta = 1/\xi \geq 1$, parameters $(B_\circ, b_a, b_r)$, $\nu = 1 - \eta^{-1/3}$, and $a = B_\circ/\big(1 + \frac{1}{3}\left(b_r - b_a\right)\big)$, with which

$$p_\phi\left[\eta\right] = a\eta^{2/3}\left(\eta \mathrm{e}^{b_r\nu} - \ \mathrm{e}^{b_a\nu}\right) \tag{41}$$

The extension here is to permit the compression to be a function of both density and temperature, as follows. On the zero–temperature isotherm, we let the compression be $\eta_\circ = v_\circ/v = \rho/\rho_\circ$. For temperatures above zero we construct the function $\eta\left[\eta_\circ,T\right]$ such that

$$\eta\left[\eta_\circ,T\right] = \eta_\circ + \left(1-\eta_n\right)\left(\eta_n/\eta_\circ\right)^{p_z}\mathrm{e}^{\eta_n-\eta_\circ} \tag{42}$$

$$\eta_n\left[T\right] = v_\circ/v_n \tag{43}$$

$$p_z = \left(v_\circ/v_c\right)^2/\left(1 - v_\circ/v_c\right) \tag{44}$$

Figure 3 illustrates the function η used in (41), and which has the asymptotic property $\lim_{\eta_\circ \to \infty} \eta = \eta_\circ$. The exponent p_z is chosen so that in the limit $T \to T_c$ the derivative $\partial\eta/\partial\eta_n = 0$ in order to avoid a singularity described shortly.

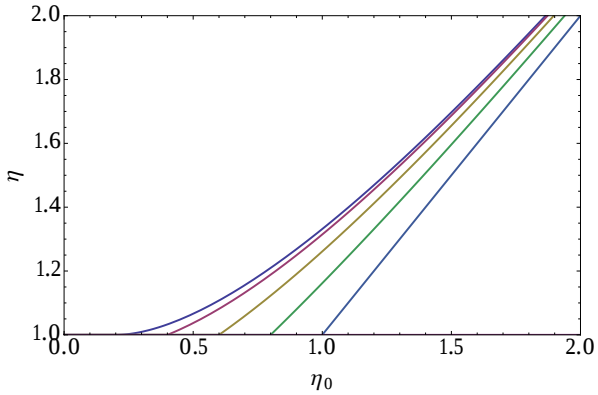

Figure 3. The function $\eta\,[\eta_\circ, T]$. Plotted for values of $\eta_n\,[T] = (0.2, 0.4, 0.6, 0.8, 1.0)$.

This usage of the Barnes pressure formula in (13) has an upper limit that is temperature dependent. Hence the derivative for the condensed–phase contribution to the pressure must be evaluated with some care. In particular we find

$$\begin{aligned} -\frac{\partial e_\phi}{\partial v} &= \frac{\partial}{\partial v} v_\circ \int_1^\xi p_\phi\,[\tilde{\eta}]\, d\tilde{\xi} \\ &= v_\circ p_\phi\,[\eta]\, \frac{\partial \xi}{\partial v} \\ &= p_\phi\,[\eta]\, \frac{\partial \xi}{\partial \xi_\circ} \end{aligned} \tag{45}$$

in which the second line follows by use of Leibnitz's rule; and the third line follows because $\xi_\circ = 1/\eta_\circ$. Similarly we have

$$\begin{aligned} \frac{\partial e_\phi}{\partial T} &= -\frac{\partial}{\partial T} v_\circ \int_1^\xi p_\phi\,[\tilde{\eta}]\, d\tilde{\xi} \\ &= -v_\circ p_\phi\,[\eta]\, \frac{\partial \xi}{\partial T} \\ &= -v_\circ p_\phi\,[\eta]\, \frac{\partial \xi}{\partial \xi_n} \frac{\partial \xi_n}{\partial T} \\ &= -v_\circ p_\phi\,[\eta]\, \frac{\partial \xi}{\partial \xi_n} \left(-\frac{\rho_\circ}{\eta^2} \frac{\partial \rho_n}{\partial T} \right) \end{aligned} \tag{46}$$

which is needed for evaluation of the condensed–phase contribution to the energy in (16). Note that the derivative $\partial\rho_n/\partial T$ is infinite at the critical point, which is why it is that we require the function (42) to have the property $\partial\xi/\partial\xi_n = (\eta_n/\eta)^2 \partial\eta/\partial\eta_n = 0$ for $T \to T_c$.

D. Patches

Here we describe four different patches to the EOS functions that are necessitated either by Maxwell's construction or by pathologies that arise when computing second derivatives of the Helmholtz free energy (13). Each of these patches is designed to be a solution to a particular problem; the efficacy of the solution is measured by how the thermodynamic consistence may be affected. Thermodynamic consistency is a relationship between the thermal and caloric EOS given by

$$\frac{\partial e}{\partial v} + p - T\frac{\partial p}{\partial T} = 0 \tag{47}$$

which is, in terms of F,

$$\frac{\partial F}{\partial v} + T\frac{\partial}{\partial v}\left(-\frac{\partial F}{\partial T}\right) + \left(-\frac{\partial F}{\partial v}\right) - T\frac{\partial}{\partial T}\left(-\frac{\partial F}{\partial v}\right) = 0 \tag{48}$$

and the equality will hold provided that the order of differentiation can be reversed, which is always true when the differentiation is analytic. Hence any EOS derived from a Helmholtz free energy will automatically satisfy (47). Because our treatment of Region III is a parameterized version of Maxwell's construction, consistency will be only approximate there; the accuracy of which is made quantitative in § III D.

The first patch is required due to introducing the coexistence region by means of the parameterized Maxwell's construction. In Region IV condition (47) is satisfied by setting the thermal part of the pressure (equation (14) second term) equal to $p_s\,[T]$. Then the thermal part of the energy (equation (16) second term) is

$$e\,[v_n, T] + \left(T\frac{\partial p_s}{\partial T} - p_s\right)(v - v_n) \tag{49}$$

which is the exact integral of (47) because both the derivative, and the saturation pressure, are constants.

The second patch is needed because $\partial e/\partial T$ can become negative at low temperatures in Region II. In this region there is only a thermal contribution. The remedy is to use a cut–off procedure on temperature, using an additional input parameter c_4, as follows. For $T/T_c < c_4$ we compute the pressure p_4 and energy e_4 on the saturation curve and temperature $T_4 = c_4 T_c$:

$$p_4 = p[v_g[T_4], T_4] \tag{50}$$

$$e_4 = e[v_g[T_4], T_4] \tag{51}$$

and for Region II points such that $T < T_4$ and $v > v_g$ we use the perfect gas relations

$$p[v,T] = p_4\,(T/T_4)\,(v_4/v) \tag{52}$$

$$e[v,T] = e_4\,(T/T_4) \tag{53}$$

with which consistency (47) is satisfied exactly.

The third patch is needed because the condensed–phase part of $\partial e/\partial T$ can become negative at large compressions in Region IV. The remedy is to simply evaluate $\partial\eta/\partial\eta_n$ in (46) at $T = T_c$. This formally destroys consistency in Region IV in favor of retaining physical values for the derivatives. The penalty for this approximation is shown in later figures where we plot the literal value of the normalized consistency defined in § III E.

The fourth and final (so far) patch is introduced for safety's sake, and it covers an extremely small part of the $[v,T]$ phase space. This is a small slice of isotherms that pass through the critical point, where the slope of the saturation curve is infinite. Whereas we have taken care to mitigate the effects of this singularity, we believe that it is safer to use a preemptive measure to ensure that a pathological energy derivative will not be computed there. The safety remedy is to multiply the energy correction (49) by the factor $1 - 2H_\circ[T/T_c, 50]$ which removes the correction in a tiny slice of temperature space at and slightly below the critical temperature.

III. DETERMINATION OF SUBSTANCE–SPECIFIC PARAMETERS

Here we begin the process of finding the substance–specific parameters by fitting the MGGB EOS to the data in the Sesame tabular database. For any substance, the Sesame data for pressure and internal energy are stored in a two–dimensional array of discrete values of density–temperature space (ρ_i, T_j), such that $(1 \le i \le \mathrm{NR}, 1 \le j \le \mathrm{NT})$, where (NR,NT) are the array dimensions. Data for constant j are isotherms and data for constant i are isochores. For increasing i and j the density and temperature increase. The next three sections detail the means by which parameters are found; particular values of the parameters are summarized in Appendix D. A summary of the "goodness–of–fit" is given in Appendix E where the root–mean–square (RMS) difference between the MGGB fit and the Sesame data is displayed on a region–by–region basis.

A. Energy at Low Density

For the first fitting exercise, we extract Sesame data for energy and pressure, $e\left[\rho_1, T_j\right]$ and $p\left[\rho_1, T_j\right]$, at the lowest nonzero isochore (which is sometimes $i = 1$ and sometimes $i = 2$, depending on the particular Sesame table). We call this data the "low" density data because ρ_1 is small compared to $\rho_\circ$, and we let $v_\infty = 1/\rho_1$. We also let $e_\circ = e\left[\rho_1, T_1\right]$, if $T_1 = 0$, and use an extrapolation to zero temperature otherwise.

Figure 4 plots the low density data compared to the MGGB functions for Sesame 7150 Water. The first coefficient to be found is c_1, used in (22), which controls the magnitude of the upward energy shift in the thermal energy $e - e_\circ$, plotted by the dashed curve. The coefficient c_2 establishes the fit to the low temperature pressure. Coefficients (Θ_1, d_1) control the centering temperature and width of the numerical Heavyside function $H_\circ$ in (22); these parameters determine the location and width of the bump that is exhibited in both the Sesame data and the MGGB fit (solid line). Parameters (Θ_2, d_2) control the centering temperature and width of the $H_\circ$ appearing in (23).

Thus the function $C\left[\tau\right]$, used in (18–19), plays the role of a low–density specific heat, which increases from some constant value at low temperature to a higher constant value at high temperature; representing the energetics of dissociation and ionization. The function $\Gamma_\circ\left[T\right]$ plays the role of a quantity like $(\gamma - 1)$; it increases from c_2 at temperatures far below Θ_2 to a value of two–thirds at temperatures far above Θ_2. This is supposed to represent the change in the internal degrees of freedom as the substance approaches a fully ionized state at high temperature.

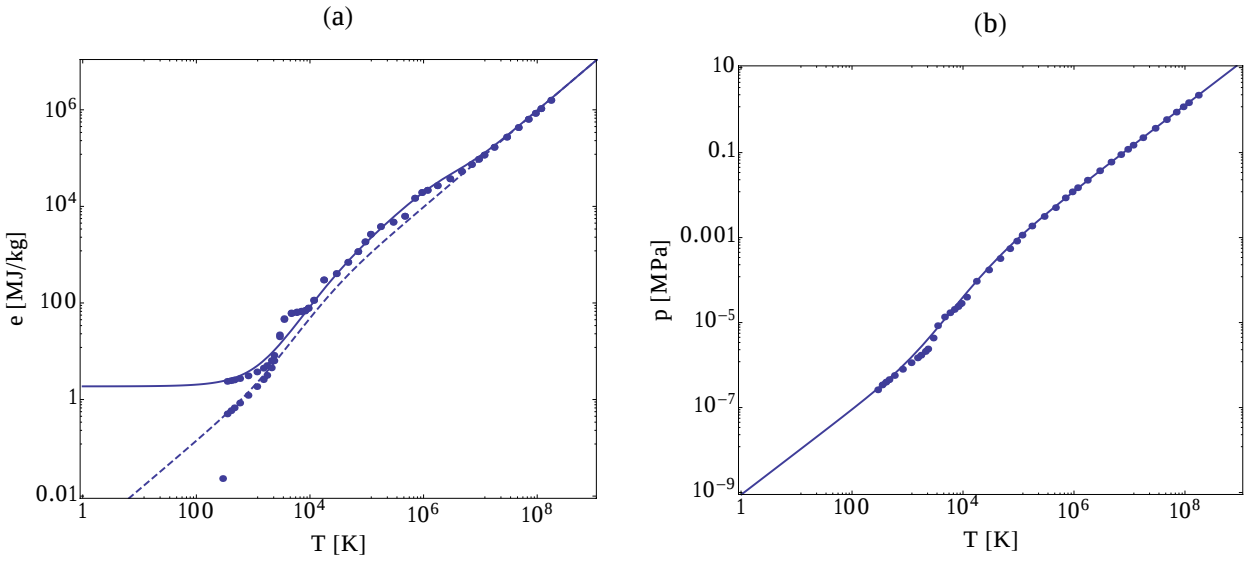

Figure 4. MGGB fit to the "zero" density data for Sesame 7150 Water. (a) $e\left[v_\infty, T\right]$; (b) $p\left[v_\infty, T\right]$; in both plots, symbols are the Sesame data. In (a) data for both e and $e - e_\circ$ are shown; dashed line is the MGGB fit for the energy evaluated using $\Theta = 1$, which removes the effect of the scaling temperature.

Clearly the MGGB fit is an approximation to the Sesame data, which has the effect of smoothing over some of the physical detail such as the dissociation of water shown here. The goodness of this fit varies with the particular substance considered. A quantitative measure of the smoothing is given in Appendix E, where we display the RMS difference between MGGB and the Sesame tabular data, on a region–by–region basis, for dry air, water, methane, aluminum, copper, and tungsten.

B. Pressure at Zero Temperature

Substance–specific values of $(B_\circ, b_r, b_a)$ are determined from the so–called Sesame cold curve $p\,[\rho_i, T_1]$, where the value of T_1 is typically zero (or at least a very low value). In most cases this is a simple matter of finding the values originally used in the EOS table construction process. Therefore, we regard $(B_\circ, b_r, b_a)$ as being given directly by the Sesame data. For water the fit is shown in Fig. 5. In this case it is likely that the Sesame cold curve pressure was generated by a function nearly identical to the Barnes[3] expression used here, although the means by which the transition into Region IV at higher temperatures is unknown.

For most of the materials studied in this report, the value of bulk modulus $B_\circ$ at normal conditions is typically given in the Sesame Handbook.[4] Given $B_\circ$, the other two parameters are found using a function fitting routine in *Mathematica*,[17] called `FindFit`, which finds parameters that minimize the RMS difference between a functional and specified data. Here, the specified data are the cold curve pressures at and above the normal density $\rho_\circ$.

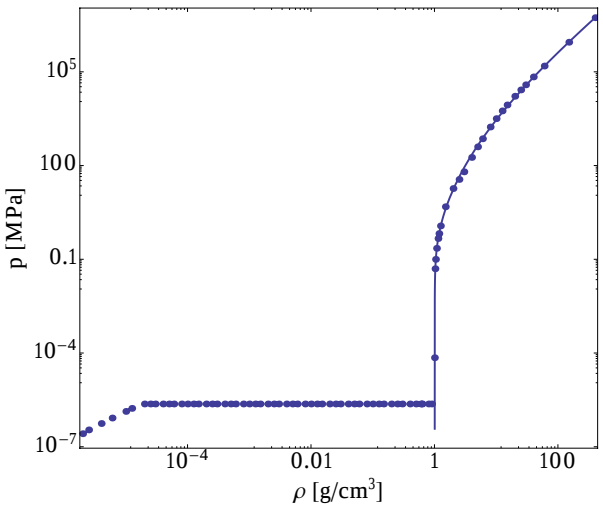

Figure 5. MGGB fit to the "zero" temperature pressure data (cold curve) for Sesame 7150 Water. Symbols are the Sesame data for $T = 290.121$ K, which is the lowest isotherm in the tabular data.

Unfortunately not every Sesame EOS table was generated using the Barnes formula for $p_\phi[\eta]$, however, the preponderance of the tables were. The table for dry air, for example, clearly did not use the Barnes form and the fit is not nearly as good as for others that did use it. The quantitative measure of the goodness of fit is given in the RMS differences displayed for Regions IV & V in Appendix E.

C. Coexistence

Measured data for the density of saturated vapor, saturated liquid, saturation pressure, and latent heat are summarized for a large collection of substances in a handy reference by Vargaftik.[5] When the corresponding Sesame table contains the phase–coexistence region, it is (typically) gauged to fit the measured data as well. Hence, we find that fitting measured data is essentially the same as fitting the Sesame data, when it exists.

The MGGB parameters (q, r, ρ_z) control the fit of the saturation curve to the data. For water the result is shown in Fig. 6. Similar accuracy is obtained for dry air and for methane, both of which have data in the Vargaftik handbook.

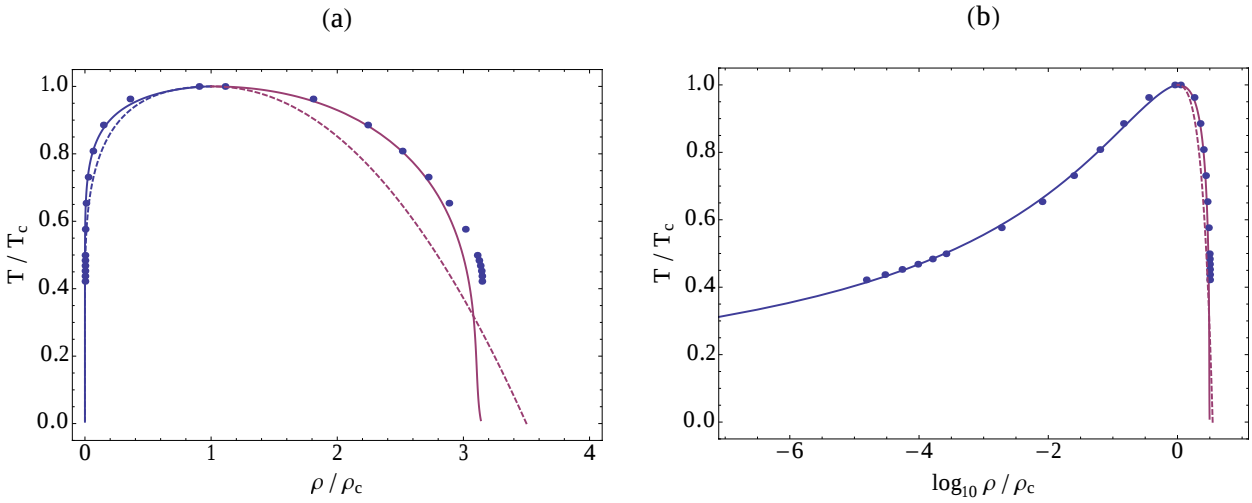

Figure 6. MGGB fit to the saturation density data of Vargaftik[5] for water. (a) Linear scale; (b) Log–Linear scale; in both plots symbols are the Vargaftik data; solid line is the MGGB fit for water; dashed lines show the "universal" saturation curve from Figure 2.

Figure 6 illustrates the reason that we go to all the trouble of using the extra shaping parameter ζ in (32–34); the MGGB fit to the data is quite good, while the universal curve, which is associated with materials obeying the Principle of Corresponding States, does not fit the data at all. This is supposed to be due to the fact that the water molecule is a polar one, to which the Principle does not apply. For methane (a nonpolar molecule) the universal curve fits the data well; hence we apply the universal curve parameters to methane, aluminum, copper and tungsten, assuming that they all obey Principle outlined by Guggenheim.[2]

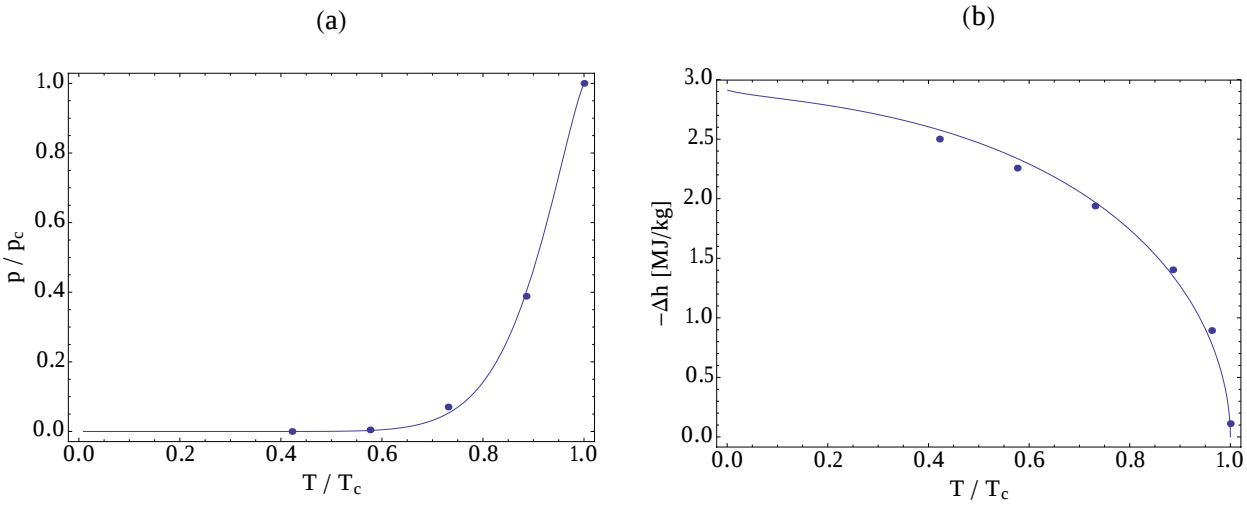

Figure 7. MGGB fit to the saturation pressure and latent heat data of Vargaftik[5] for water. (a) saturation pressure; (b) latent heat; in both plots symbols are the Vargaftik data.

The MGGB saturation pressure and critical pressure $p_c = p\,[v_c, T_c]$ are controlled by the parameters (c_3, d_3, d_4, α); and the latent heat is controlled by the parameter σ. The fitting result for water is shown in Fig. 7; with similar accuracy found for dry air and methane.

When the Sesame EOS does not contain the coexistence region, either via Maxwell's construction or otherwise, MGGB inserts one; in which case, the Sesame data for energy at the density of saturated condensed–phase is used to determine the value of the latent heat parameter σ. In those cases for which this procedure is used, the parameter is generally very close to that for a substance that obeys the Principle of Corresponding States. According to Guggenheim,[2] for such a substance the value of $-\Delta h/\hat{R}T = 9.05$ at $T/T_c = 0.57$ (where $\hat{R} = R/\hat{M}$). When data are not available that establish the condensed–phase energy, we assume that this condition holds exactly, which determines σ. For materials that are not expected to obey the Principle of Corresponding States, such as water, then the experimental data are relied upon entirely for finding σ. The result is that the value of T/T_c for which $-\Delta h/\hat{R}T = 9.05$ will be different from 0.57, as is shown in Fig. 8.

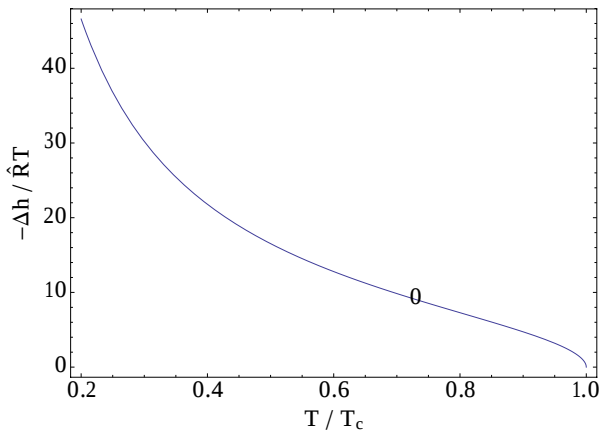

Figure 8. MGGB fit for the latent heat of water. The symbol shows the value of T/T_c for which $-\Delta h/\hat{R}T = 9.05$.

D. Sesame Comparison

The next figures furnish a graphical comparison of the MGGB EOS with the corresponding Sesame EOS. First for Sesame 7150 Water:

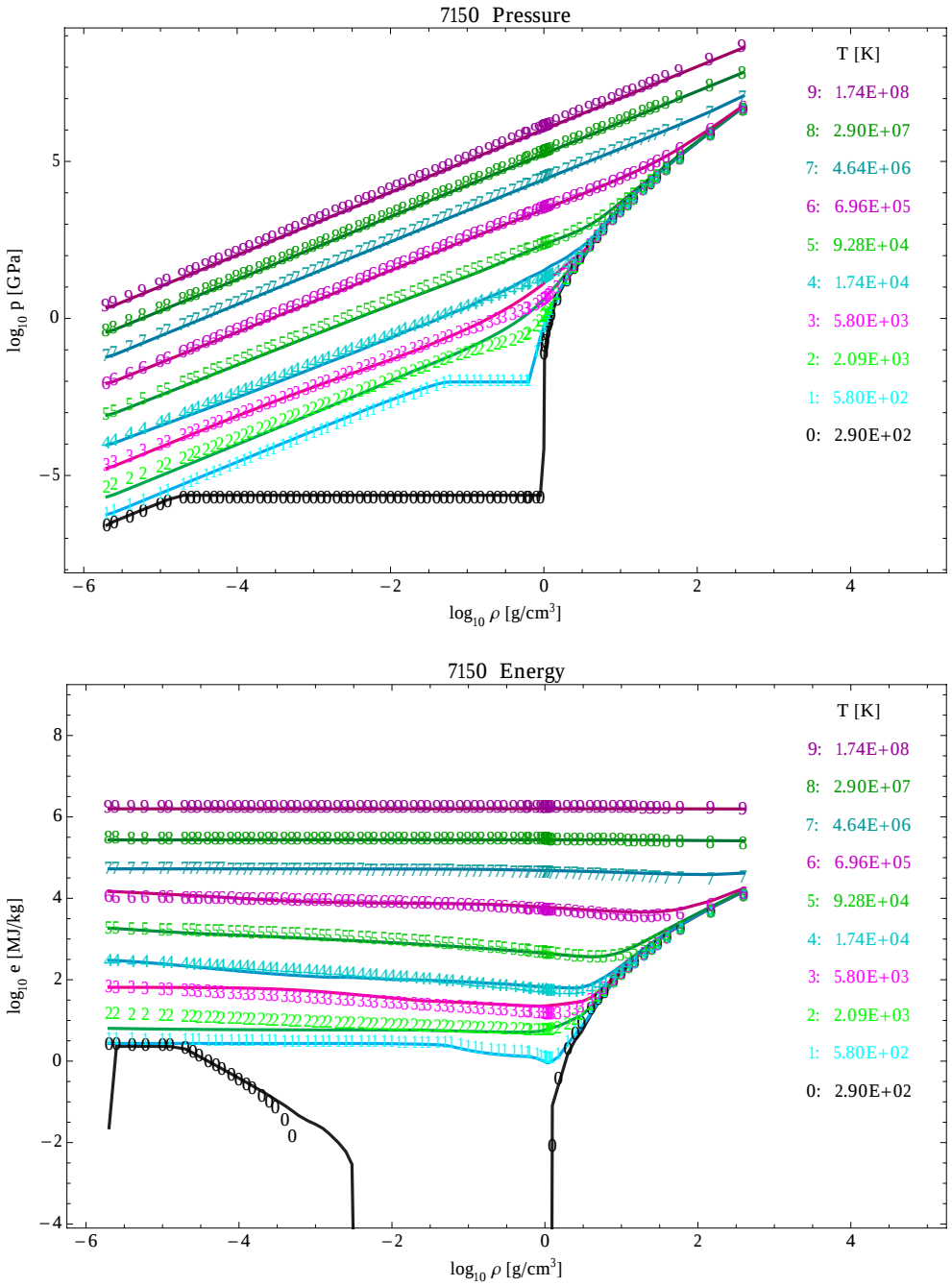

Figure 9. Comparison of the MGGB fit to Sesame 7150 Water. Top $p\,[v,T]$; bottom $e\,[v,T]$; solid line connects the Sesame tabular data points; symbols mark the MGGB fit evaluated at the Sesame $[v,T]$ points.

and second, for Sesame 3336 Copper:

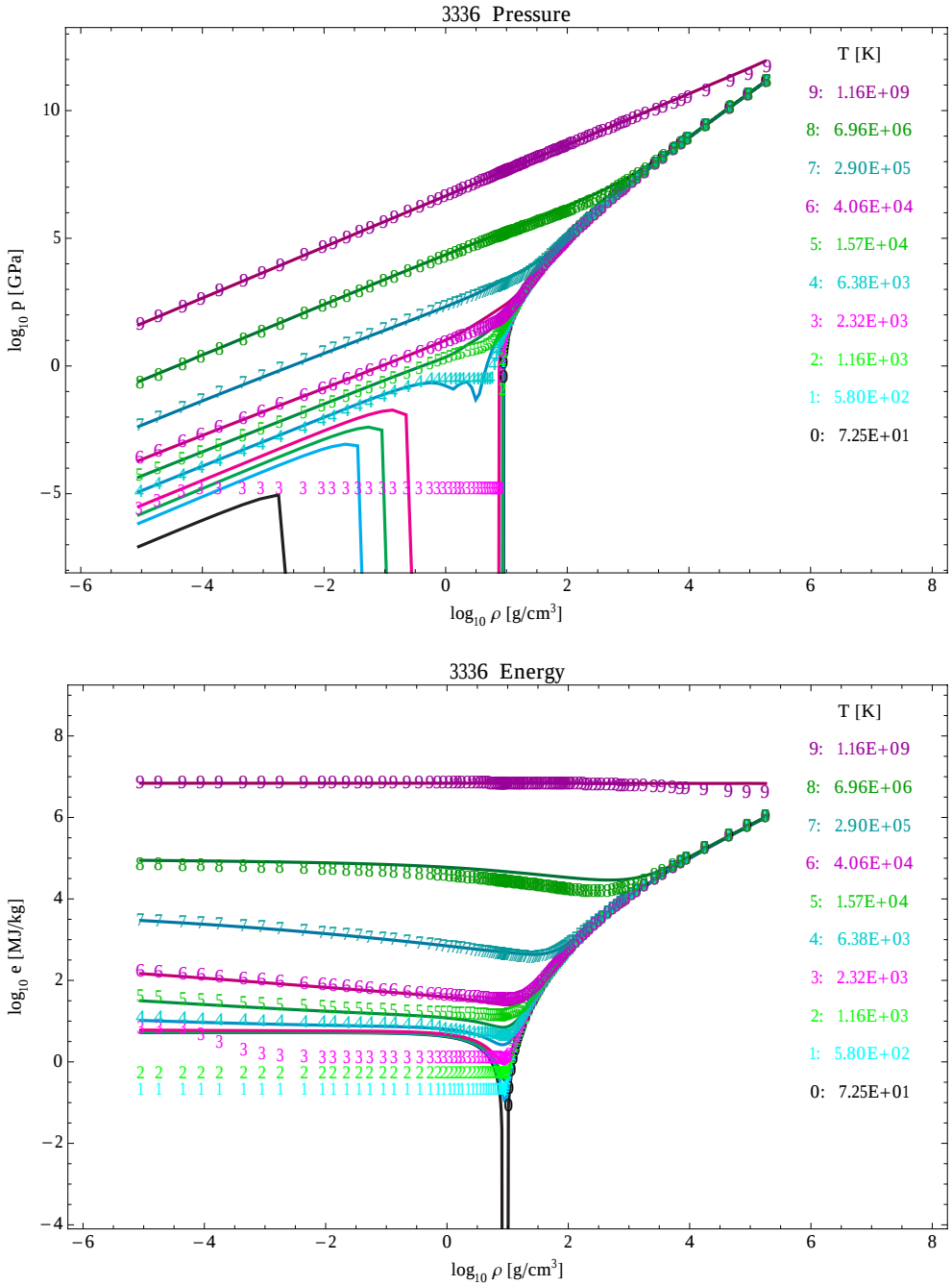

Figure 10. Comparison of the MGGB fit to Sesame 3336 Copper. Top $p\,[v,T]$; bottom $e\,[v,T]$; solid line connects the Sesame tabular data points; symbols mark the MGGB fit evaluated at the Sesame $[v,T]$ points.

In the foregoing display the tabular Sesame data points are connected by the solid line; symbols are centered at the MGGB EOS evaluated at the Sesame points $[\rho_i, T_j]$ for selected isotherms as marked in the figures. The quantitative differences are given in Appendix E. Figure 9 shows that when a coexistence region exists in the Sesame data, the MGGB EOS reproduces it well; further, the fit is generally good everywhere except just above the critical point where the MGGB pressure tends to be low. Because this is an area of $[v,T]$ space for

which there is considerable uncertainty anyway, we do not regard the difference as being a flaw in the MGGB formulae.

In the case of copper, shown in Fig. 10, the Sesame EOS does not contain the coexistence region; and the one exhibited by the MGGB EOS is plausible in the sense that the data for all regions except for Region III appear to overlap well.

E. Derivatives

Between the thermal EOS $p\,[v,T]$ and the caloric EOS $e\,[v,T]$ there are four derivatives; given the condition (47) only three of them are independent. These derivatives appear in the definition of four measurable quantities. Using the classical symbol for each quantity they are[18]

$$\kappa \equiv -\frac{1}{v}\left(\frac{\partial v}{\partial p}\right)_T \quad : \text{constant temperature compressibility} \tag{54}$$

$$\beta \equiv \kappa\left(\frac{\partial p}{\partial T}\right)_v = \frac{1}{v}\left(\frac{\partial v}{\partial T}\right)_p \quad : \text{constant pressure expansivity} \tag{55}$$

$$\eta \equiv -\left(\frac{\partial T}{\partial v}\right)_e = \frac{1}{c_v}\left(\frac{\partial e}{\partial v}\right)_T \quad : \text{Joule coefficient} \tag{56}$$

$$c_v \equiv \left(\frac{\partial e}{\partial T}\right)_v \quad : \text{constant volume specific heat} \tag{57}$$

(Note: the classical symbol η used for the Joule coefficient is not to be confused with the compression.) In that which follows we use these classical symbols to carry the derivative data, with the exception of the first energy derivative for which we use the symbol $e_{,v} \equiv (\partial e/\partial v)_T$.

In the coexistence region, where the pressure is constant on isotherms, the derivative $(\partial p/\partial v)_T$ is zero; so the compressibility is, literally, infinite. For the purposes of numerical integration of multifield problems, this is not very helpful. Because the mixture compressibility is presumably finite there, we define a "physical" one simply as the mass–weighted average of the compressibility on the saturation curve. That is, for any temperature we compute $\kappa_g\,[T]$ and $\kappa_n\,[T]$ on the saturation curve and for any point in the coexistence region we let

$$\begin{aligned} \kappa\,[v,T] &= \mathrm{f}\kappa_n + (1-\mathrm{f})\kappa_g \\ \mathrm{f} &= \left(\frac{1/v - 1/v_g}{1/v_n - 1/v_g}\right) \end{aligned} \tag{58}$$

In a similar fashion we define the expansivity in the coexistence region by evaluating $\beta_g[T]$ and $\beta_n[T]$ on the saturation curve and for any point in the coexistence region we let

$$\beta[v,T] = \mathrm{f}\beta_n + (1-\mathrm{f})\beta_g \tag{59}$$

using the same interpolant f. In what follows we will refer to the foregoing κ and β as the "physical" derivatives, in contrast to those which would be computed directly from the EOS which we will call the "literal" derivatives. Note that the physical and literal derivatives are the same everywhere except in Region III.

For a perfect gas $\kappa = 1/p$ and $\beta = 1/T$, so it is natural to plot κp and βT; thus, both quantities will have a unit value in regions for which the material may be well represented by a perfect gas. The consistency condition (47) is $1 + e_{,v}/p = (T/p)(\partial p/\partial T)_v$. Thus, it is natural to plot the function $1 + e_{,v}/p$, which we will call the "Joule Function"; a quantity that should be greater than zero and has a unit value for a perfect gas. In the figure that follows, the specific heat is normalized by the constant value $C_\circ = 3R/\hat{M}$. Using these normalizations, the derivatives for MGGB Water are plotted in Fig. 11; the same plots for all six test materials are displayed in Appendix E.

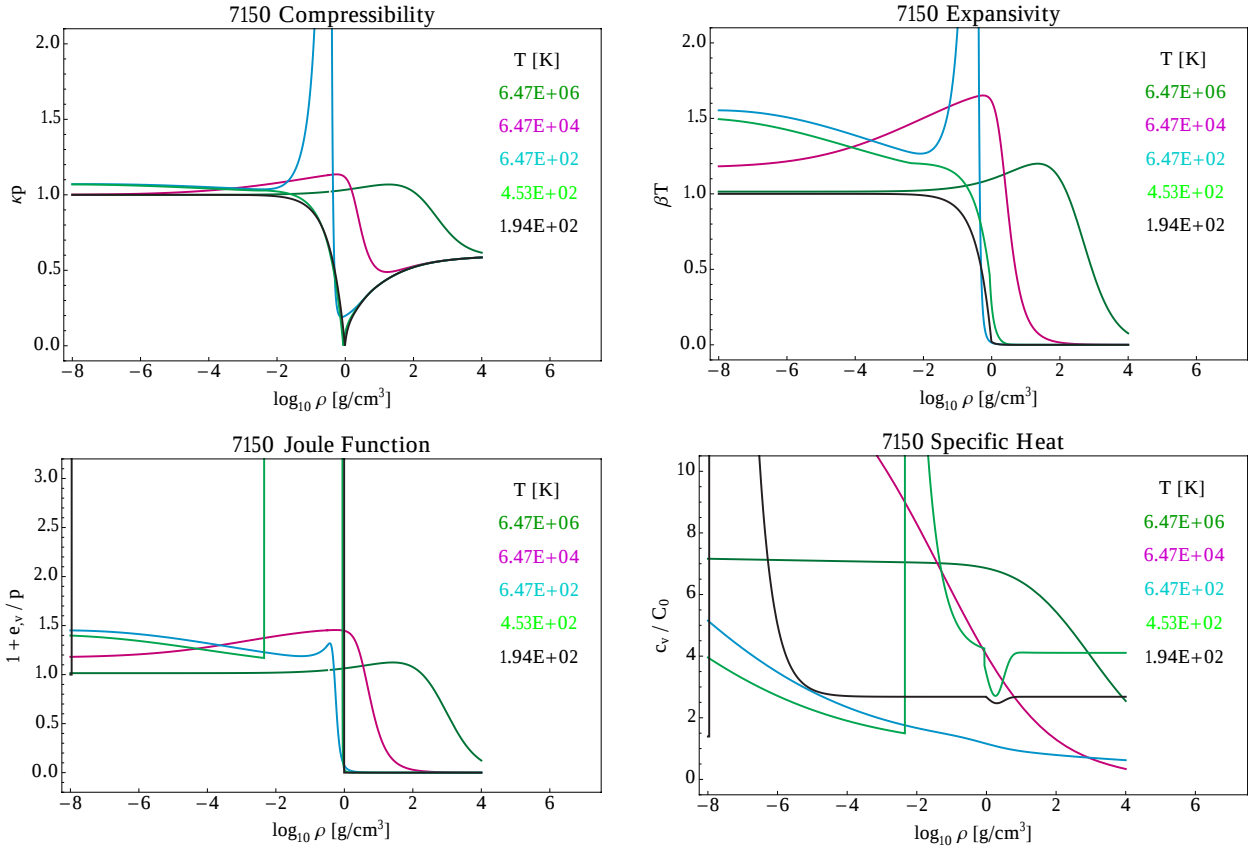

Figure 11. Derivatives for MGGB 7150 Water. Compressibility and Expansivity are the physical derivatives; Joule Function and Specific Heat are both literal derivatives.

The plots in Fig. 11 are furnished in order to illustrate the fact that the physical κ and β make a sensible transition between perfect gas behavior at low

density and temperature and highly nonperfect behavior at high temperature and high density. Furthermore, the values are finite and nonnegative everywhere, including the coexistence region, which is important for obtaining sensible numerical solutions using the specific volume evolution expressed in (10). The literal values for Joule Function and specific heat are likewise sensible insofar as they are both positive; these are necessary for use in the model equations for energy (5).

The ratio of specific heats γ appears prominently in the wave theory of gas dynamics. For $\gamma \geq 0$ the gas dynamic equations are hyperbolic.[19] In Fig. 12 we use the identity

$$\gamma\left[v,T\right]=\frac{c_p}{c_v}=\frac{\left(\partial p/\partial v\right)_s}{\left(\partial p/\partial v\right)_T}=\frac{c^2\kappa}{v} \tag{60}$$

where we use the physical values for κ. The sound speed c is given by the isentropic derivative

$$c^2\left[v,T\right]\equiv\left(\frac{\partial p}{\partial \rho}\right)_s=\frac{v}{\kappa}+v^2\left(\frac{p+e_{,v}}{c_v}\right)\frac{\beta}{\kappa} \tag{61}$$

where we again use the physical κ and β, and the literal $e_{,v}$ and c_v. Our normalization of the sound speed is c^2/pv, which is identical to γ for a perfect gas.

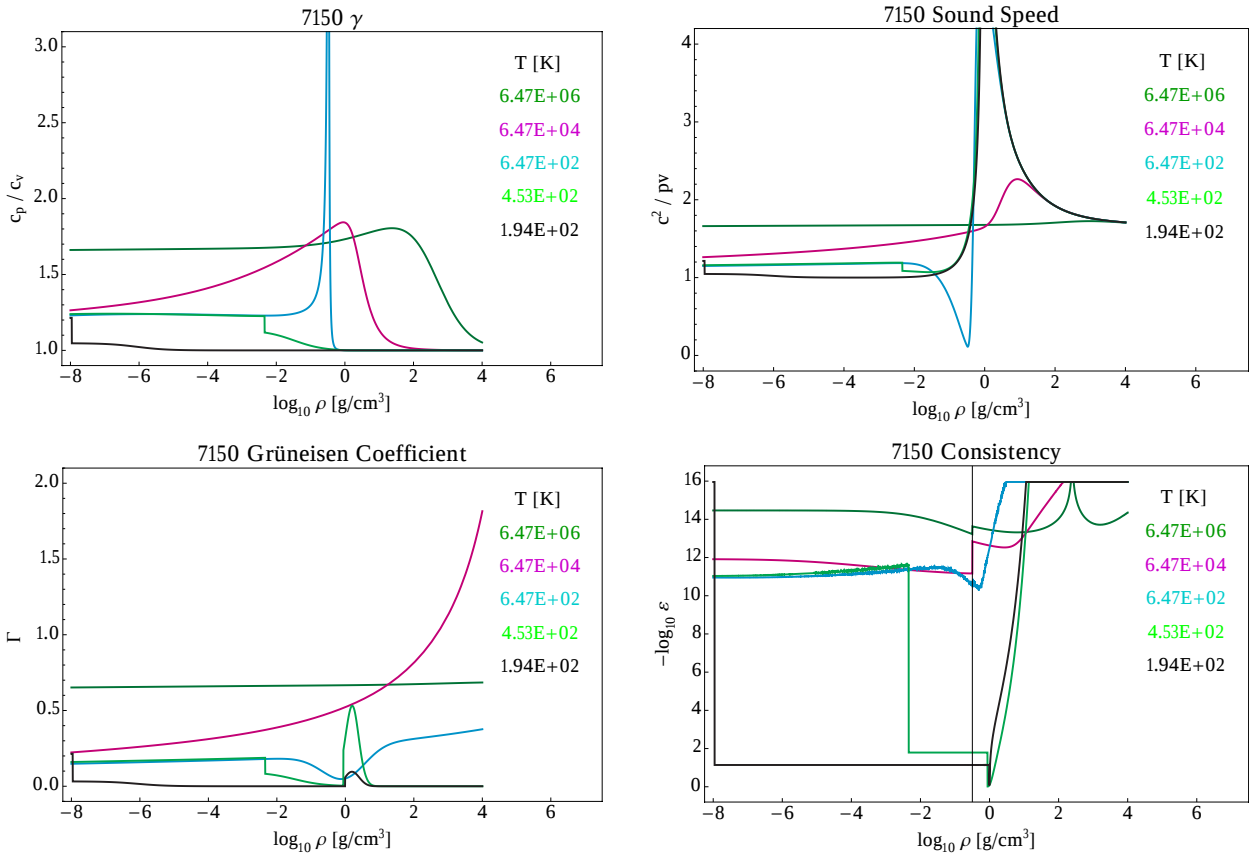

Figure 12. Derivatives for MGGB 7150 Water. γ, c^2, Γ and normalized consistency ε.

In Fig. 12 we also plot the so–called Grüneisen coefficient

$$\Gamma\left[v,T\right] \equiv v\left(\frac{\partial p}{\partial e}\right)_v = v\frac{\left(\partial p/\partial T\right)_v}{\left(\partial e/\partial T\right)_v} \tag{62}$$

using only literal derivatives. Recall the condition for thermodynamic consistency (47), whose locally normalized residual, squared, is

$$\varepsilon\left[v,T\right] \equiv \frac{\left(e_{,v}+p-T\partial p/\partial T\right)^2}{\left(e_{,v}\right)^2+p^2+\left(T\partial p/\partial T\right)^2} \tag{63}$$

in which only literal derivatives are used, and for which we plot $-\log_{10}\varepsilon$; this estimates the number of digits in the normalized residual. (So that larger values indicate "more consistency.")

Values of γ, c^2 and Γ exhibit the kind of variation to be expected over the full range of temperature–density space. The consistency (which is limited to 16 digits) is good everywhere except in Region III, where it is only fair. This is a result of the approximation used to represent Maxwell's construction, and varies from material to material. Generally the one to two digit consistency shown there is judged to be acceptable.

F. Isentropes and Hugoniots

Let $T_S\left[v\right]$ be the temperature at specific volume v for which the isentropic expression

$$de\left[v,T_S\right] + p\left[v,T_S\right]\ dv = 0 \tag{64}$$

is satisfied. The level curves $e\left[v,T_S\right]$ and $p\left[v,T_S\right]$ are called isentropes. A particular isentrope is found by integration of (64) in v, using a specified point $[v,T]$ as an initial condition. The next figure (Figure 13) shows selected isentropes for water, using both the MGGB fit and the Sesame data.

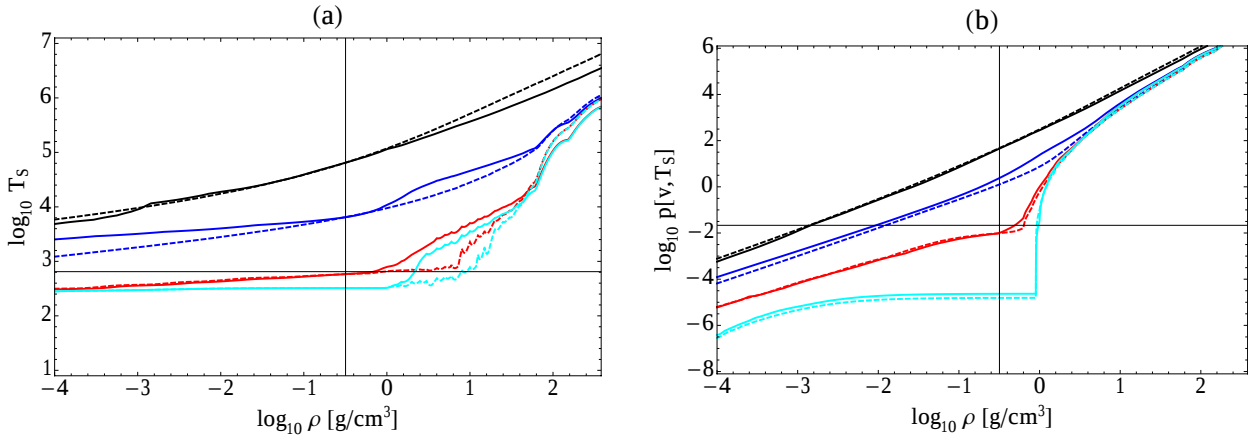

Figure 13. Isentropes comparing the MGGB fit to Sesame 7150 Water. (a) $T_S\left[v\right]$; (b) $p\left[v,T_S\right]$; solid lines are for Sesame 7150 Water; dashed lines are for the MGGB fit; in both plots, the axes origin is the critical point; curves are for isentropes passing through four points: Black$[v_c, 100T_c]$; Blue$[v_c, 10T_c]$; Red$[v_c, 0.9T_c]$; Cyan$[v_c, 0.5T_c]$.

Clearly the temperature is not a constant on isentropes, so the pressure isentrope is not an isotherm. The nature of pressure isentropes indicates certain features of solutions to wave problems using the corresponding EOS. In this regard, the fundamental derivative in gas dynamics $\mathcal{G}$ is helpful; again using c for the isentropic sound speed, $\mathcal{G}$ is defined

$$\mathcal{G} = \frac{1}{c}\frac{\partial \rho c}{\partial \rho} \tag{65}$$

According to Menikoff,[19] when $\mathcal{G} > 0$ the sound modes of the gas–dynamic equations are linearly non–degenerate: compressive waves steepen to form shocks and expansive waves spread out to form rarefactions. This is the physical case of interest. The derivative $\mathcal{G}$ is a measure of convexity of pressure isentropes; and the Grüneisen Coefficient Γ is a measure of their spacing; for $\Gamma > 0$ isentropes do not intersect.[19] Convexity is difficult to observe in Fig. 12. The subcritical curves exhibit a cusp on the condensed–phase side of the saturation curve; on the high density side it is difficult to see if they may intersect. The next figure (Figure 14), which displays $\mathcal{G}\,[v, T_S]$ and $\Gamma\,[v, T_S]$ corresponding to the isentropes in Fig. 13, shows that the pressure isentropes are indeed convex and that they are nonintersecting (although they come very close, as indicated by the very small values of Γ on the low temperature isotherm). Note that on the lowest isotherm the convexity is essentially zero, corresponding to the very flat pressure isotherm in the coexistence region where the isentropic sound speed is very small, in which case our numerical evaluation of $\mathcal{G}$ becomes noisy.

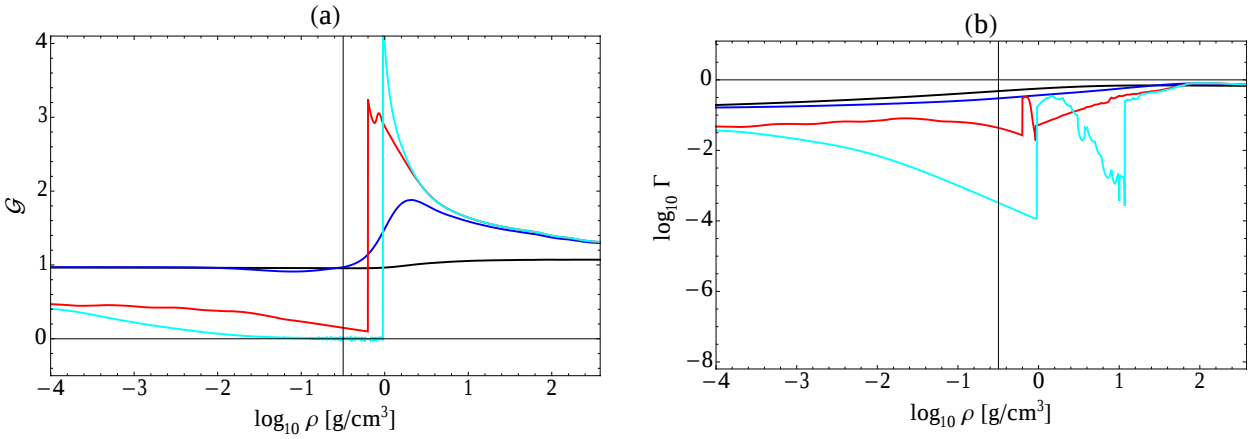

Figure 14. $\mathcal{G}$ and Γ for the MGGB fit to Sesame 7150 Water. (a) $\mathcal{G}\,[v, T_S]$; (b) $\Gamma\,[v, T_S]$; curves are for isentropes passing through four points: Black$[v_c, 100T_c]$; Blue$[v_c, 10T_c]$; Red$[v_c, 0.9T_c]$; Cyan$[v_c, 0.5T_c]$; axes origin passes through the critical density.

Using subscripts (L, R) for the uniform conditions to the left and right of a steady one–dimensional compression wave moving with speed U, the closed conservation laws can be expressed:

$$-U\left(\rho_{R}-\rho_{L}\right)+\left(\rho_{R}u_{R}-\rho_{L}u_{L}\right)=0 \tag{66}$$

$$\left(u_{R}-u_{L}\right)^{2}+\left(p_{R}-p_{L}\right)\left(v_{R}-v_{L}\right)=0 \tag{67}$$

$$\left(e_{R}-e_{L}\right)+\tfrac{1}{2}\left(p_{R}+p_{L}\right)\left(v_{R}-v_{L}\right)=0 \tag{68}$$

$$p_{L}-\tilde{p}[v_{L},T_{L}]=0 \tag{69}$$

$$e_{L}-\tilde{e}[v_{L},T_{L}]=0 \tag{70}$$

a system commonly called the "Hugoniot relations." When conditions are specified on the right side, say, these are five equations in the unknown left side state $(\rho_{L},u_{L},e_{L},p_{L},T_{L})$ plus the wave speed U. Hence, if any element of the state, or the wave speed itself, is specified, then the Hugoniot relations determine all of the other unknowns. When the left side velocity is specified such that $u_{L}=u_{p}$, and the right side velocity is zero, then the problem is that of a piston moving toward a stationary medium, which generates a shock wave moving with speed $U=u_{s}$ into the medium. The curve defined by $u_{s}\left[u_{p}\right]$ is often referred to simply as the "Hugoniot." These curves are plotted here for both the MGGB fit and for Sesame 7150 Water (Figure 15).

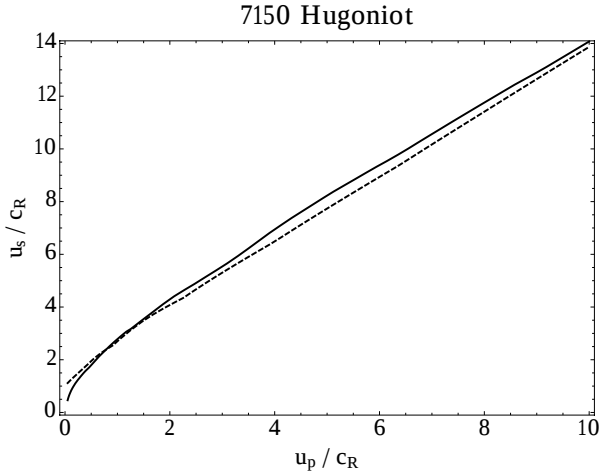

Figure 15. Hugoniot comparing MGGB fit to Sesame 7150 Water. Conditions to the right are $(p_{R},T_{R})=(1\text{ bar},300\text{ K})$; speeds are normalized by the right side isentropic sound speed c_{R}; solid line is the Sesame 7150 Water EOS; dashed line is the corresponding MGGB EOS.

The slope of the $u_{s}\left[u_{p}\right]$ curve is usually found experimentally by observing the shock wave generated in a sample of material by the impact of a projectile from a gas gun. The Sesame data are typically gauged in order to reproduce this experimental data; note that the MGGB result reproduces the Sesame data. The accuracy of this agreement is almost wholly dependent on the accuracy of the cold curve pressure/energy agreement; which is quite good in this particular case.

In the limit of zero piston speed, the shock speed should be the isentropic sound speed $c_{_R}$, corresponding to an infinitely weak wave. Hence, the Hugoniot curve should go to $u_s/c_{_R} = 1$ for $u_p/c_{_R} = 0$ which appears to be true for MGGB but not for Sesame 7150 Water. This difference is of little significance in problems for which the principal interest is the effects of strong shocks. However, when the waves are weak this difference could lead to difficulties in obtaining robust numerical solutions. (As a general rule numerical solutions are more robust when they mimic the physical behavior of the system studied. In this case the compression waves are entropy–increasing ones, and the amount of entropy produced in the physical waves is a stabilizing factor in the forward–time numerical solution of the wave dynamics. When the entropy–production is underestimated by a flawed EOS, the stability of the numerical solution can become poor.)

IV. NUMERICAL EVALUATION OF THE MULTIFIELD EOS

A. The Semi–Equilibrium Case

We use Newton's iterative method to find the solution to (1–3) in such a way that the volume condition (1) is satisfied at every iteration. Using $\rho_{\rm r} = M_{\rm r}/V$, and $(f, g_{\rm r}, h_{\rm r})$ for the $2N_{\rm f}+1$ residuals of (1–3), we have

$$f = 1 - \sum \rho_{\rm r} v_{\rm r} \tag{71}$$

$$g_{\rm r} = \tilde{p}_{\rm r}[v_{\rm r}, T_{\rm r}] - p \tag{72}$$

$$h_{\rm r} = \tilde{e}_{\rm r}[v_{\rm r}, T_{\rm r}] - e_{\rm r} \tag{73}$$

where the sum over all fields is understood. We seek changes in pressure, volume, and temperature $(\Delta p, \Delta v_{\rm r}, \Delta T_{\rm r})$ such that values of $(p, v_{\rm r}, T_{\rm r})$ used for the next iteration will produce residuals of reduced magnitude. [Important remark: We find that using the physical derivatives is very helpful in stabilizing the iteration; the literal derivatives (for which κ and β are infinite) are pathological, which is destabilizing.] The residuals will go exactly to zero if the functions are linear and the changes are given by the system

$$-f = -\sum \rho_{\rm r} \Delta v_{\rm r} \tag{74}$$

$$-g_{\rm r} = -\frac{1}{v_{\rm r}\kappa_{\rm r}} \Delta v_{\rm r} + \frac{\beta_{\rm r}}{\kappa_{\rm r}} \Delta T_{\rm r} - \Delta p \tag{75}$$

$$-h_{\rm r} = e_{,v{\rm r}} \Delta v_{\rm r} + c_{v{\rm r}} \Delta T_{\rm r} \tag{76}$$

where all functions are evaluated explicitly using data for the current iteration. This is Newton's method. One can readily solve this system for the changes by eliminating Δp as follows. By solving (76) for $\Delta T_{\rm r}$ and placing the result in (75) and using (74) with $f = 0$, we find that

$$p^+ = p + \Delta p = \frac{\sum \rho_{\rm r} \left(a_{\rm r} \tilde{p}_{\rm r} - b_{\rm r} h_{\rm r} / c_{v{\rm r}} \right)}{\sum \rho_{\rm r} a_{\rm r}} \tag{77}$$

where p^+ is the next–iterate value, and where we use $\eta_{\rm r} = e_{,v{\rm r}}/c_{v{\rm r}}$ in the coefficients

$$a_{\rm r} = \kappa_{\rm r} / \left(1/v_{\rm r} + \beta_{\rm r} \eta_{\rm r} \right) \tag{78}$$

$$b_{\rm r} = \beta_{\rm r} / \left(1/v_{\rm r} + \beta_{\rm r} \eta_{\rm r} \right) \tag{79}$$

Using $g_{\rm r}^+$ to signify (72) with p replaced by p^+ we have

$$\Delta v_{\rm r} = a_{\rm r} g_{\rm r}^+ - b_{\rm r} h_{\rm r} / c_{v{\rm r}} \tag{80}$$

$$\Delta T_{\rm r} = - \left(h_{\rm r} + \eta_{\rm r} \Delta v_{\rm r} \right) \tag{81}$$

Whereas the EOS functions for $\tilde{p}$ and $\tilde{e}$ are continuous in the dependent variables $[v, T]$, the derivatives can possess very large discontinuities. Because the trial solution depends on these derivatives, some care must be taken to prevent excessive excursion in the trial solution during the iteration. For this we resort to a trick used by Ramshaw & Chang[20] for analogous nonlinear root finding problems using Newton's method. The trick is to limit the changes so the largest change is of such a nature that the resulting value of $v_{\rm r}$ or $T_{\rm r}$ is, at least, nonnegative. This is ensured by applying a multiplicative limiter μ to each of the changes. We use

$$\mu = {\rm Max} \left[1, -2\Delta_{min}, \Delta_{max} \right]^{-1} \tag{82}$$

where

$$\Delta_{min} = {\rm Min} \left[0, \Delta v_{\rm r}/v_{\rm r}, \Delta T_{\rm r}/T_{\rm r} \right] \tag{83}$$

$$\Delta_{max} = {\rm Max} \left[1, \Delta v_{\rm r}/v_{\rm r}, \Delta T_{\rm r}/T_{\rm r} \right] \tag{84}$$

which limits the largest decrease in value to be one that cuts the value in half; and also (just for the sake of robustness) it limits the largest increase to one that doubles the current value. The effect of the limiter is to under–relax the Newton iteration when at least one of the $2N_{\rm f}+1$ elements is far from the solution, while using a literal Newton iteration otherwise.

B. The Full–Equilibrium Case

In this case condition (1) is replaced by one involving a single temperature, and the condition (3) is replaced by a single expression involving the mass–mean EOS energy. Hence we now have the $N_{\rm f}+2$ residuals

$$f = 1 - \sum \rho_{\rm r} v_{\rm r} \tag{85}$$

$$g_{\rm r} = \tilde{p}_{\rm r}[v_{\rm r}, T] - p \tag{86}$$

$$h = \sum \rho_{\rm r} \tilde{e}[v_{\rm r}, T] - \sum \rho_{\rm r} e_{\rm r} \tag{87}$$

and the changes for Newton's iteration are given by the solution to the linear system

$$-f = -\sum \rho_{\rm r} \Delta v_{\rm r} \tag{88}$$

$$-g_{\rm r} = -\frac{1}{v_{\rm r}\kappa_{\rm r}} \Delta v_{\rm r} + \frac{\beta_{\rm r}}{\kappa_{\rm r}} \Delta T - \Delta p \tag{89}$$

$$-h = \sum \rho_{\rm r} \left(e_{,v{\rm r}} \Delta v_{\rm r} + c_{v{\rm r}} \Delta T \right) \tag{90}$$

Using g^+ to signify (86) with p replaced by p^+ we have from (89)

$$\Delta v_{\rm r} = v_{\rm r} \left(\kappa_{\rm r} g_{\rm r}^+ + \beta_{\rm r} \Delta T \right) \tag{91}$$

which can be used in (90) to obtain

$$\Delta T = -(h/b) - \sum a_{\rm r} g_{\rm r}^+ \tag{92}$$

where

$$b = \sum \rho_{\rm r} c_{v{\rm r}} \left(\eta_{\rm r} v_{\rm r} \beta_{\rm r} + 1 \right) \tag{93}$$

$$a_{\rm r} = \rho_{\rm r} c_{v{\rm r}} \eta_{\rm r} v_{\rm r} \kappa_{\rm r} / b \tag{94}$$

By combining (92) and (89), and using (88) with $f = 0$, we have the next–iterate pressure

$$p^+ = \frac{\sum_{\rm r} \rho_{\rm r} v_{\rm r} \kappa_{\rm r} \tilde{p}_{\rm r} + \sum_{\rm r} \rho_{\rm r} v_{\rm r} \beta_{\rm r} \sum_{\rm s} a_{\rm s} \tilde{p}_{\rm s} - (h/b) \sum_{\rm r} \rho_{\rm r} v_{\rm r} \beta_{\rm r}}{\sum_{\rm r} \rho_{\rm r} v_{\rm r} \kappa_{\rm r} + \sum_{\rm r} \rho_{\rm r} v_{\rm r} \beta_{\rm r} \sum_{\rm s} a_{\rm s}} \tag{95}$$

which is to be used to replace p in (86) so that the volume changes are ones that exactly satisfy the volume condition at every iteration. And again, because of the potentially large variation in the derivatives, robustness is improved by use of the limiter μ to prevent catastrophic excursions in the trial solution.

V. FURTHER WORK

There are two main areas in which users of the MGGB EOS could benefit from follow on work. One area is the formulation of the fitting functions, and the other is computational evaluation of the functions.

With respect to the fitting functions there are a number of improvements and extensions that could be pursued. One is the addition of a contribution to (13) due to free electrons. In terms of Sesame data this would require an additional function that fits the ionization table, in order to determine the free electron number density. Another improvement could be found by performing a more detailed evaluation of the equations defining Maxwell's construction (39–40), so that the saturation curve consistent with (13) can be found more accurately. This would improve the consistency in Region III.

Computer evaluation of the MGGB EOS requires a great deal more operations on the Central Processing Unit (CPU) than for, say, a perfect gas EOS or interpolation in a tabular database. This is the CPU cost of doing more detailed physics over a full–range of $[v, T]$ space. The main value obtained from doing this CPU work is to retrieve good physical derivatives of the EOS, which are required for multifield applications. It may be possible to tabulate these derivatives along with the thermal and caloric EOS, and thereby achieve satisfactory results at a much lower CPU cost. Because the density of data in the tabular database determines how well the EOS is rendered, it could be profitable to build the table during the calculation. In this way a high resolution of the EOS data could be maintained in the region of $[v, T]$ space associated with the particular problem of interest.

There are certainly other areas of improvement that will likely become apparent as the MGGB EOS is put into practice, and which are not anticipated here. For those future investigators who may wish to make repairs, explore improvements, and install extensions, the *Mathematica*[17] notebooks used in this work can be made available.

ACKNOWLEDGMENTS

Los Alamos National Laboratory is operated by Los Alamos National Security LLC, for the U.S. Department of Energy's National Nuclear Security Administration under contract DE–AC52-06NA25396. Support from both DOE/NNSA, and the U.S. Department of Defense, is gratefully acknowledged.

We thank Eugene Symbalisty for bringing to our attention the particular application motivating this work, and for his patience with us in getting the work done; we also thank Ralph Menikoff for occasional consultation on certain theoretical underpinnings used throughout the work; we thank Scott Crockett for reading the manuscript; and we *really* thank Jack and Joanne Barnes for not only having coined the term "Sesame," but for having played a crucial role in making the term stand for a high level of technical excellence — permitting Sesame to serve innumerable applications so well, and for so long.

REFERENCES

[1]E. Grüneisen, "Zustand des festen körpers," (Julius Springer Verlag, 1926) Chap. 1 in *Handbuch der Physik*, edited by H. Geiger and K. Scheel, p. 22.
[2]E. A. Guggenheim, Journal of Chemical Physics **13**, 253 (1945).
[3]J. F. Barnes, Physical Review **153**, 269 (1967).
[4]*T-4 Handbook of Material Properties Data Bases, Vol. Ic: Equations of State*, edited by K. S. Holian, LA–10160–MS (Los Alamos National Laboratory, 1984).
[5]N. B. Vargaftik, *Tables on the Thermophysical Properties of Liquids and Gases*, 2nd ed. (Hemisphere, 1975).
[6]B. A. Kashiwa and L. M. Hull, in *7th Joint Classified Bombs/Warheads & Ballistics Symposium* (National Defense Industrial Association, 2004).
[7]B. A. Kashiwa and L. M. Hull, Journal of Energetic Materials, In press (2010).
[8]T. D. Sewell and R. Menikoff, in *APS Topical Conference, Shock Compression of Condensed Matter, Portland, OR, July 20–25* (2003).
[9]H. C. Graboske, "A New EOS for Air," Internal Report UCID–16901 (Lawrence Livermore Laboratory, 1976).
[10]F. H. Ree, "Equation of State of Water," Internal Report UCID–52190 (Lawrence Livermore Laboratory, 1976).
[11]G. I. Kerley, J. Appl. Phys. **51**, 5368 (1980).
[12]K. Trainor, "A New Full–Range Equation of State for Aluminum," Internal Report UCID–18574–82–2 (Lawrence Livermore Laboratory, 1982).
[13]K. Trainor, J. Appl. Phys. **54**, 2372 (1983).
[14]B. Bennett, "SESAME #3541: Tungsten," (Los Alamos Scientific Laboratory, 1979) Chap. 3541 in *T–4 Handbook of Material Properties Data Bases*[4], pp. 3541/1–6.
[15]E. D. Chisolm, S. D. Crockett and D. C. Wallace, Physical Review B **68**, 104103 (2003).
[16]O. K. Rice, "Critical phenomena," (Princeton University Press, 1955) Chap. E in *Thermodynamics and Physics of Matter*, edited by F. D. Rossini, p. 419.
[17]S. Wolfram, *The Mathematica Book* (Cambridge University Press, 1988).
[18]F. D. Rossini, *Thermophysics and Physics of Matter* (Princeton University Press, 1955).
[19]R. Menikoff, "Numerical implication of riemann problem theory for fluid dynamics," Internal Report LA–UR–88–2672 (Los Alamos National Laboratory, 1988).
[20]J. D. Ramshaw and C. H. Chang, Journal of Computational Physics **116**, 359 (1995).
[21]*Mathematical Handbook for Scientists and Engineers*, 2nd ed., edited by G. A. Korn and T. M. Korn (McGraw–Hill, 1961).

Appendix A: Handy Functions

The logarithmic Heaviside function used in this report is defined

$$H_\circ[x,d] = \tfrac{1}{2}\big(1 + \mathrm{Erf}[d\log x]\big) \tag{A1}$$

The first derivative, normalized to a unit value at $x = 1$, is

$$H_1[x,d] = \frac{x\sqrt{\pi}}{d}\frac{\partial H_\circ}{\partial x} = \mathrm{e}^{-(d\log x)^2} \tag{A2}$$

These two functions look like this

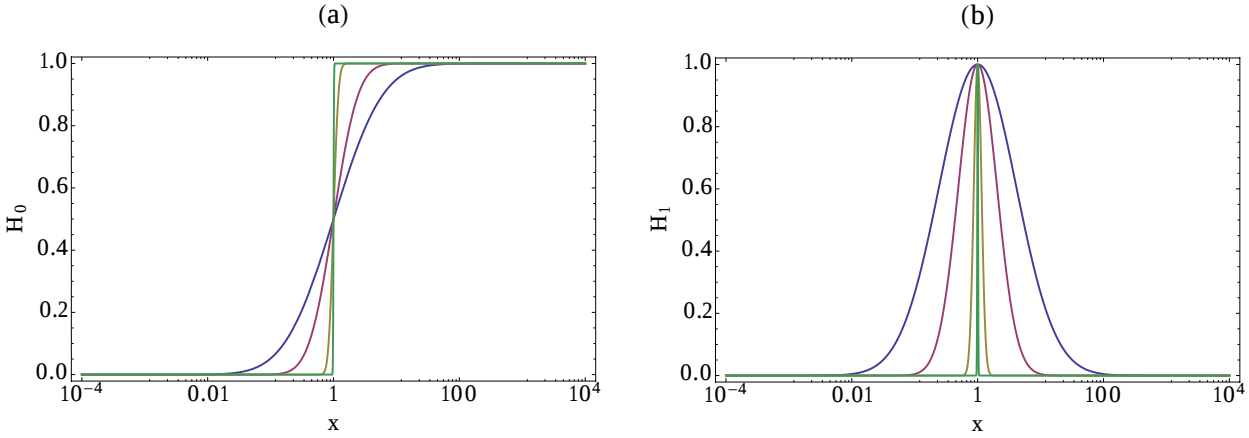

Figure A1. Logarithmic Heavyside and Delta functions. (a) $H_\circ[x,d]$; (b) $H_1[x,d]$; increasingly sharper curves correspond to $d = (0.5, 1.0, 5.0, 50.)$; $H_\circ[1,d] = 1/2$; and $H_1[1,d] = 1$.

Appendix B: Dirty Tricks

Leibnitz's rule[21] for the differentiation of an integral is

$$\frac{\partial}{\partial\lambda}\int_{u(\lambda)}^{v(\lambda)} f(x,\lambda)\; dx = \int_{u(\lambda)}^{v(\lambda)} \frac{\partial}{\partial\lambda} f(x,\lambda)\; dx + f(v,\lambda)\frac{\partial v}{\partial\lambda} - f(u,\lambda)\frac{\partial u}{\partial\lambda} \tag{B1}$$

which is used for differentiation of the Helmholtz free energy. This comes into play for terms like the thermal part of (14) which contains the term

$$\begin{aligned}
-\frac{\partial}{\partial v}\left(-\Theta\int_0^{T/\Theta} C\,[\tau]\left(\frac{T}{\Theta}-\tau\right)\;\frac{d\tau}{\tau}\right) &= T\frac{\partial s_{_T}}{\partial v} - \frac{\partial\Theta e_{_T}}{\partial v} \\
&= \left(T\frac{\partial s_{_T}}{\partial v} - \Theta\frac{\partial e_{_T}}{\partial v}\right) - e_{_T}\frac{\partial\Theta}{\partial v} \\
&= \left(T\frac{\partial s_{_T}}{\partial v} - \Theta\frac{\partial e_{_T}}{\partial v}\right) - \frac{\Theta e_{_T}}{v}\frac{\partial\log\Theta}{\partial\log v}
\end{aligned} \tag{B2}$$

where the integrals are

$$e_{_T}[v,T] = \int_0^{T/\Theta} C[\tau]\ d\tau \tag{B3}$$

$$s_{_T}[v,T] = \int_0^{T/\Theta} \frac{C[\tau]}{\tau}\ d\tau \tag{B4}$$

Using Leibnitz's rule we have

$$\begin{aligned}\Theta\frac{\partial e_{_T}}{\partial v} &= \Theta\frac{\partial}{\partial v}\int_0^{T/\Theta} C[\tau]\ d\tau = \Theta C[T/\Theta]\frac{\partial T/\Theta}{\partial v}\\ T\frac{\partial s_{_T}}{\partial v} &= T\frac{\partial}{\partial v}\int_0^{T/\Theta} \frac{C[\tau]}{\tau}\ d\tau = \Theta C[T/\Theta]\frac{\partial T/\Theta}{\partial v}\end{aligned} \tag{B5}$$

so the first right side term of (B2) is exactly zero, showing that expressing the Helmholtz free energy in the form (13) is clearly a subterfuge aimed at obtaining a Mie–Grüneisen functional form for p.

Appendix C: Summary of Integrals and Derivatives

Recall the Barnes formula for the Thomas–Fermi–Dirac equation, corrected for a zero pressure at zero compression:

$$p_\phi[\eta] = a\eta^{2/3}\left(\eta \mathrm{e}^{b_r\nu} - \mathrm{e}^{b_a\nu}\right) \tag{C1}$$

where $\eta = \rho/\rho_\circ$; $\nu = 1-\eta^{-1/3}$; and $a = B_\circ/\big(1+(b_a-b_r)/3\big)$. If we let $\xi = 1/\eta$ then $\nu = 1-\xi^{1/3}$ and the integral is

$$\begin{aligned}e_\phi[v,T] &= -v_\circ\int_1^{v/v_n} p_\phi[\eta]\ d\xi\\ &= -\frac{3}{2}v_\circ a\left[\frac{2}{b_a}\mathrm{e}^{b_a\nu} + \frac{b_r\xi^{1/3}-1}{\xi^{2/3}}\mathrm{e}^{b_r\nu} + \mathrm{Ei}\left[-b_r\xi^{1/3}\right]b_r^2\mathrm{e}^{b_r}\right]_1^{v/v_n}\end{aligned} \tag{C2}$$

For $e_{_T}$ we need

$$\begin{aligned}e_{_T}[v,T] &= \Theta\int_\circ^{T/\Theta} C[\tau]\ d\tau\\ &= \Theta\int_0^{T/\Theta} C_\circ\left(1+c_1H_\circ[\tau/\Theta_1,d_1]\right)\ d\tau\\ &= \frac{1}{2}C_\circ\Theta\left[(c_1+2)\tau + \mathrm{Erf}\left[d_1\log\frac{\tau}{\Theta_1}\right]c_1\tau - \mathrm{Erf}\left[d_1\log\frac{\tau}{\Theta_1}-\frac{1}{2d_1}\right]c_1\Theta_1\mathrm{e}^{-1/4d_1^2}\right]_0^{T/\Theta}\end{aligned} \tag{C3}$$

and for $s_{_T}$ we have

$$s_{_T}\left[v,T\right] = \int_0^{T/\Theta} C\left[\tau\right]\,\frac{d\tau}{\tau}$$
$$= \frac{1}{2}C_\circ\left[(c_1+2)\log\tau + \mathrm{Erf}\left[d_1\log\frac{\tau}{\Theta_1}\right]c_1\log\frac{\tau}{\Theta_1} + \frac{c_1}{\sqrt{\pi}d_1}\mathrm{e}^{-(d_1\log\tau/\Theta_1)^2}\right]_0^{T/\Theta} \tag{C4}$$

We also need the derivatives with respect to T of (23–24), as follows:

$$\Gamma'_\circ = \frac{\partial\Gamma_\circ}{\partial T} = \left(\tfrac{2}{3}-c_2\right)\frac{d_2}{\sqrt{\pi}}\exp\left[-\left(d_2\log\left[T/\Theta_2\right]\right)^2\right] \tag{C5}$$

$$b' = \frac{\partial b}{\partial T} = -\frac{c_3 d_3}{\sqrt{\pi}}\exp\left[-\left(d_3\log\left[T/\Theta_3\right]\right)^2\right] \tag{C6}$$

Appendix D: Summary of MGGB Parameters

Here we display values of the 23 MGGB parameters found to fit the Sesame EOS data for a selection of materials. Densities are given in units of [g/cm^3]; in the normalization we use $T_\circ = 298.15$ K; $e^* = C_\circ T_\circ$; $p^* = \rho_\circ e^*$; and as before, our reference specific heat is $C_\circ = 3R/\hat{M}$. By using the nondimensional parameters listed below, the EOS units can be established by the user's choice of gas constant R. Here we have assumed the value

$$R = 8.314472 \times 10^{-3} \quad \text{[MJ/mole–K]} \tag{D1}$$

which should render the EOS in Sesame[4] the unit system (which turns out to be, in effect, [g–cm–10μs–K]).

The first table lists eight parameters taken directly from the data for the Sesame material appearing the handbook edited by Holian.[4] As noted in §III B the parameters $(B_\circ, b_r, b_a)$ were obtained by a fitting procedure (rather than by finding the exact values used for generating the Sesame table, which would not be possible in all cases anyway).

Name	Year	Number	$\hat{M}$ [g/mole]	T_c [K]	ρ_c	$\rho_\circ$	$e_\circ$ [MJ/kg]	$e_\circ/e^*$	$B_\circ$ [GPa]	$B_\circ/p^*$	b_r	b_a
Dry Air[9]	1976	5030	29.6060	1.32E+02	0.31	1.19	0.09	0.37	1.00	3.35	3.18	6.02
Water[10]	1976	7150	18.0159	6.47E+02	0.32	1.00	1.87	4.54	3.00	7.27	2.64	5.19
Methane[11]	1980	5500	16.0426	1.91E+02	0.16	0.57	0.36	0.77	1.00	3.80	1.04	3.97
Aluminum[12]	1982	3720	26.9815	5.73E+03	0.77	2.70	11.8	42.9	77.0	103.	3.42	1.90
Copper[13]	1983	3336	63.5460	7.58E+03	2.55	8.93	5.21	44.5	134.	128.	3.91	5.01
Tungsten[14]	1979	3541	183.85	1.74E+04	5.50	19.2	4.64	115.	313.	402.	6.02	-3.38

The next table has the 15 remaining MGGB parameters that were found to give the best fit to the corresponding Sesame data.

Name	Θ_1 [K]	Θ_2 [K]	c_1	c_2	c_3	c_4	d_1	d_2	d_3	d_4	α	q	r	ρ_z	σ
Air	1.19E+06	2.64E+05	8.00	0.33	0.29	0.35	0.35	0.35	0.55	0.45	0.70	4.80	0.65	1.25	1.70
Water	5.18E+04	5.18E+04	6.00	0.20	0.18	0.35	0.30	0.30	0.50	0.50	0.70	6.50	0.65	1.50	2.50
Methane	9.53E+04	1.91E+22	0.00	0.33	0.29	0.35	1.00	1.00	0.55	0.45	0.70	4.00	0.54	0.57	1.70
Aluminum	1.72E+05	1.72E+05	6.00	0.20	0.14	0.35	0.40	0.40	1.00	0.95	0.40	4.0	0.54	2.70	2.25
Copper	7.58E+05	7.58E+05	13.7	0.20	0.14	0.35	0.30	0.30	1.00	0.95	0.40	4.00	0.54	9.38	2.25
Tungsten	3.48E+06	3.48E+06	38.3	0.33	0.24	0.50	0.30	0.30	0.80	0.80	0.50	4.00	0.54	20.2	1.60

Appendix E: Summary of MGGB–Sesame Comparisons

This table displays the RMS difference between the MGGB fit and the Sesame EOS data, broken down according to the regions of $[v, T]$ space defined in Fig. 1. This is followed by a display of the EOS for each of the six materials for which MGGB parameters have been determined. To be clear, the RMS energy difference Δe is defined

$$\Delta e = \frac{1}{N} \sum_i \sum_j \frac{\left(\tilde{e}\left[v_i, T_j\right] - e\left[v_i, T_j\right]\right)^2}{\tilde{e}\left[v_i, T_j\right]^2} \tag{E1}$$

where there are N points in the region for which $\tilde{e}\left[v_i, T_j\right]$ is the Sesame EOS and $e\left[v_i, T_j\right]$ is the MGGB EOS, each evaluated at a collection of evenly Log–spaced $[v, T]$ coordinates, such that there are 50 isotherms and 50 isochores in the total range of density–temperature space of the Sesame data, for a total of 2500 $[v, T]$ points among the five regions. Determination of the region is, of course, made on the basis of the saturation curve defined by the MGGB EOS.

		Region I			Region II			Region III			Region IV			Region V		
Name	Number	Δe	Δp	N	Δe	Δp	N	Δe	Δp	N	Δe	Δp	N	Δe	Δp	N
Dry Air	5030	0.10	0.05	1950	0.00	0.00	0	0.00	0.00	0	0.00	0.00	0	0.22	0.25	550
Water	7150	0.04	0.04	1457	0.01	0.03	40	38.	0.18	45	0.06	0.07	50	0.05	0.06	893
Methane	5500	0.20	0.01	1344	0.68	0.09	270	104.	0.17	81	0.32	0.16	77	0.31	0.27	256
Aluminum	3720	0.07	0.07	660	0.08	4.16	23	1.07	1.44	366	0.71	0.01	461	0.05	0.03	990
Copper	3336	0.04	0.01	640	0.02	0.06	29	0.89	0.97	342	0.01	0.01	489	0.07	0.05	960
Tungsten	3541	0.09	0.23	672	0.02	0.69	43	1.14	0.99	761	0.11	0.01	496	0.16	0.10	528

Generally, the RMS difference is smallest in Regions I, II, and V, which is to be expected because these areas are not associated with the phase–coexistence region. The difference is greatest in Region III which is likewise to be expected, especially for aluminum, copper and tungsten, for which the Sesame EOS does not exhibit the coexistence region. In Region IV the differences are not very great except for the aluminum energy, which suggests that the location of the MGGB saturation curve is somewhat different from the one implied by the Sesame data. In the case of air, the Sesame data is all supercritical so there appear no comparisons in Regions II, III, and IV.

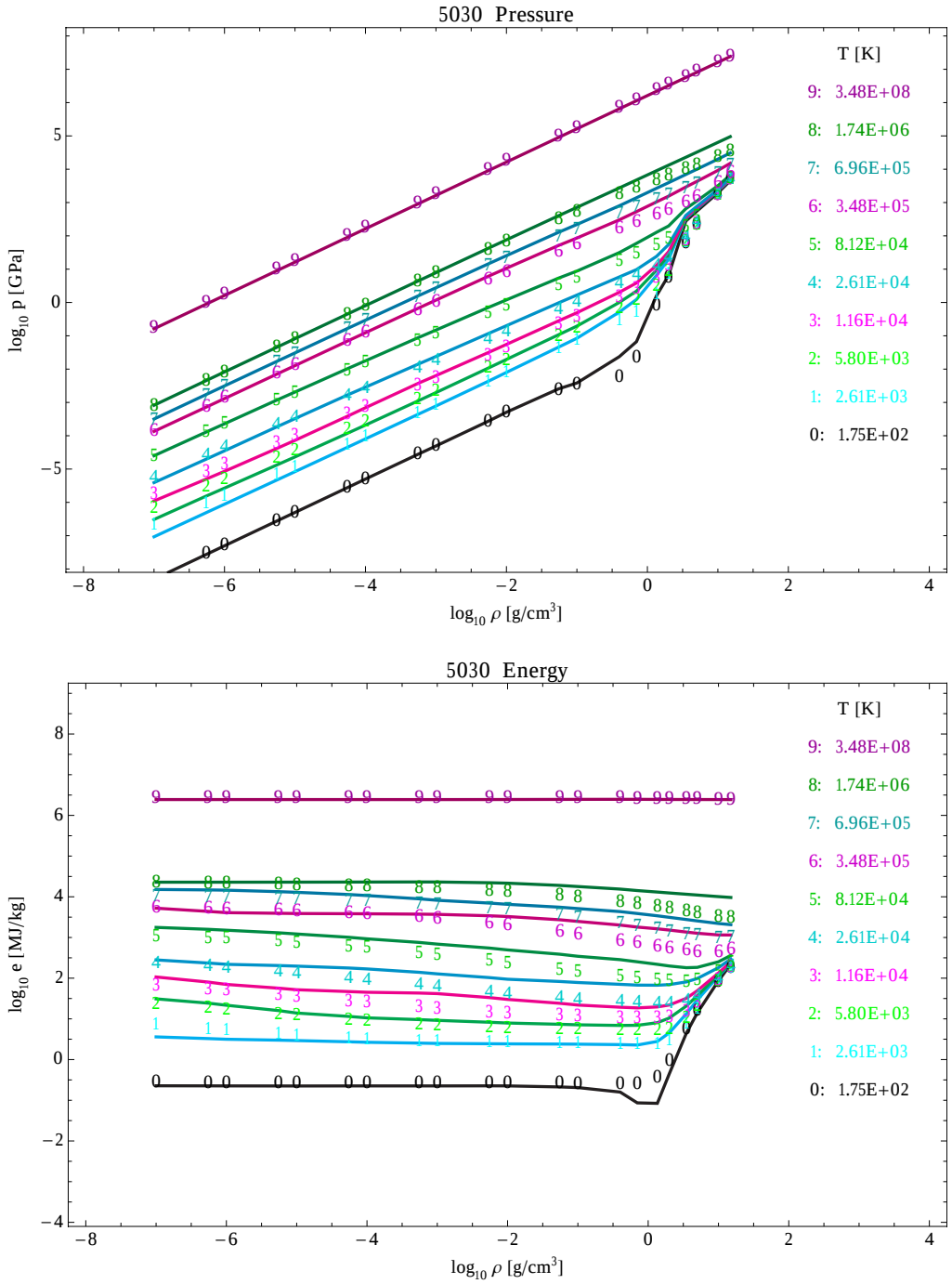

Comparison of the MGGB fit to Sesame 5030 Dry Air. Top $p\,[v,T]$; bottom $e\,[v,T]$; solid line connects the Sesame tabular data points; symbols mark the MGGB fit evaluated at the Sesame $[v,T]$ points.

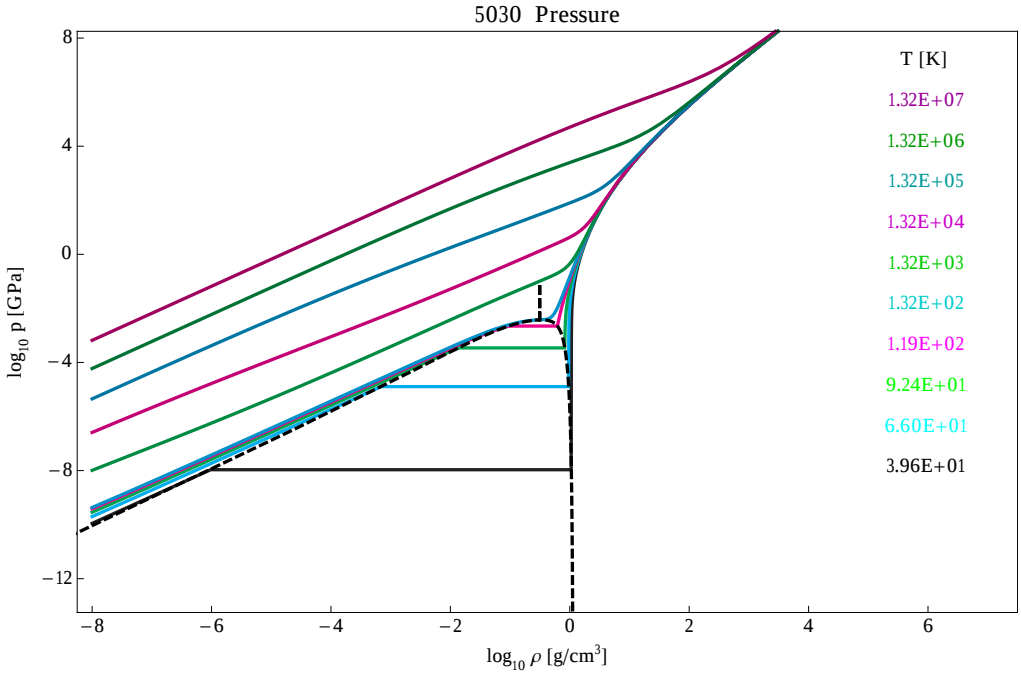

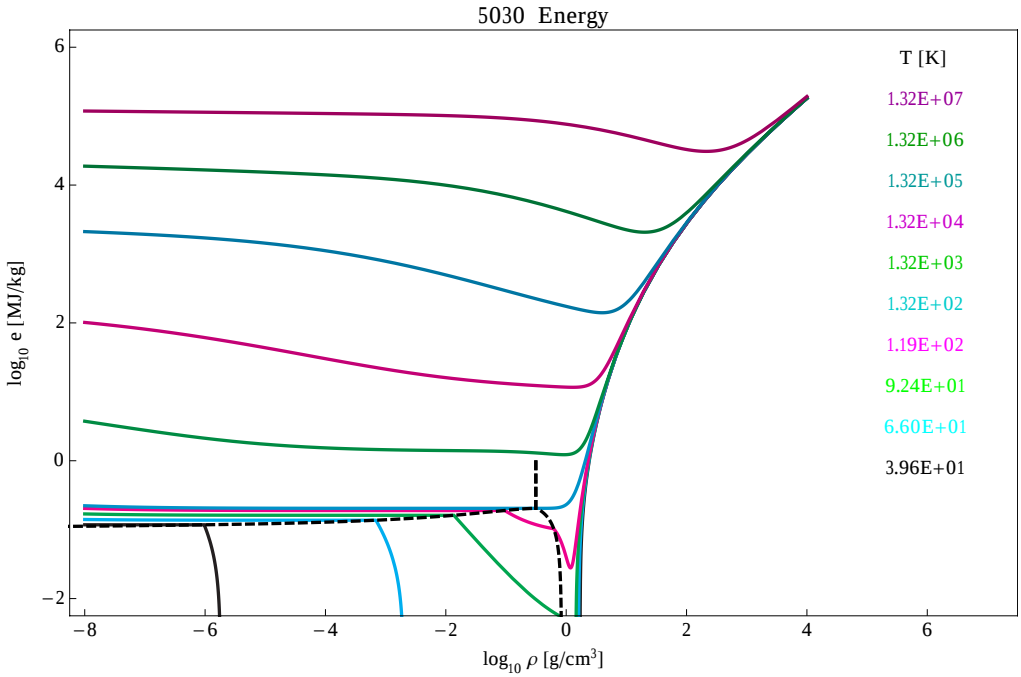

MGGB 5030 Dry Air.

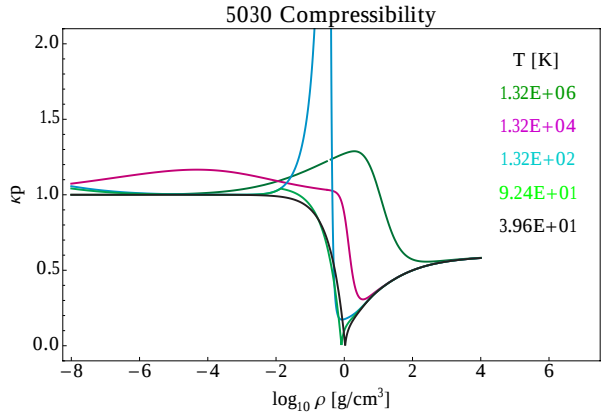
5030 Compressibility
κp
log10 ρ [g/cm3]
T [K]
1.32E+06
1.32E+04
1.32E+02
9.24E+01
3.96E+01

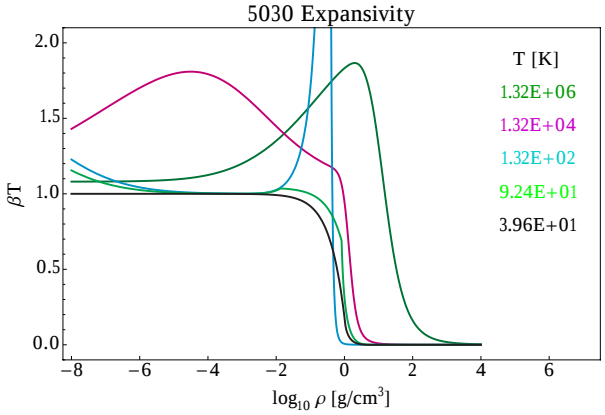
5030 Expansivity
βT
log10 ρ [g/cm3]
T [K]
1.32E+06
1.32E+04
1.32E+02
9.24E+01
3.96E+01

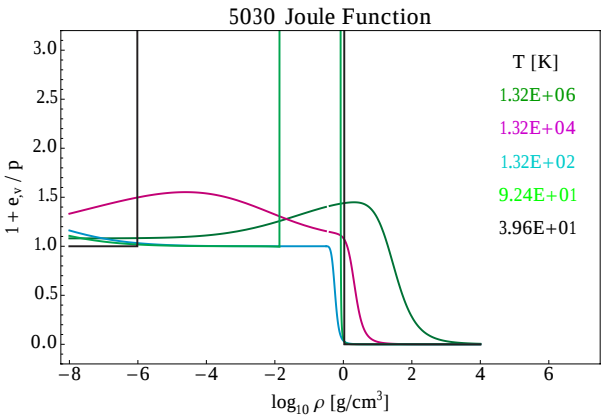
5030 Joule Function
1 + ev / p
log10 ρ [g/cm3]
T [K]
1.32E+06
1.32E+04
1.32E+02
9.24E+01
3.96E+01

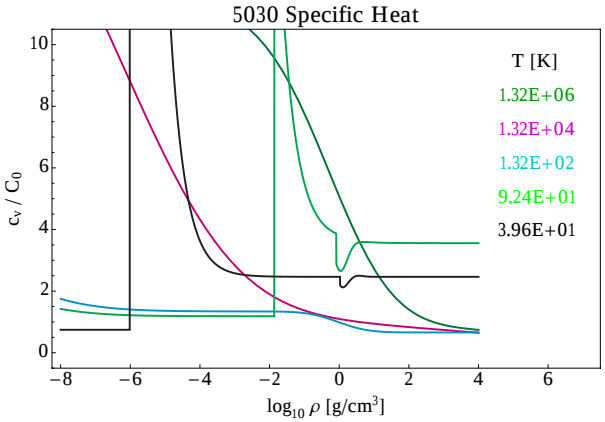
5030 Specific Heat
cv / C0
log10 ρ [g/cm3]
T [K]
1.32E+06
1.32E+04
1.32E+02
9.24E+01
3.96E+01

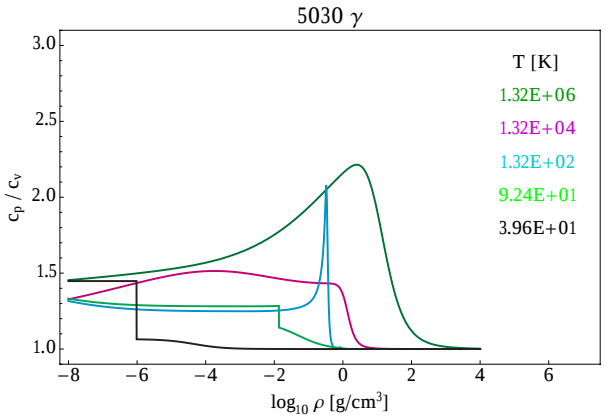
5030 γ
cp / cv
log10 ρ [g/cm3]
T [K]
1.32E+06
1.32E+04
1.32E+02
9.24E+01
3.96E+01

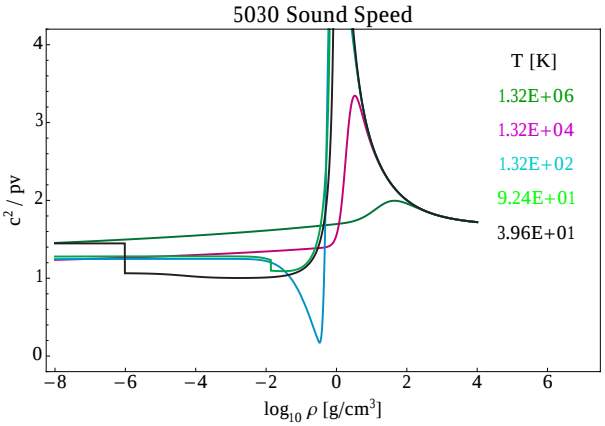
5030 Sound Speed
c2 / pv
log10 ρ [g/cm3]
T [K]
1.32E+06
1.32E+04
1.32E+02
9.24E+01
3.96E+01

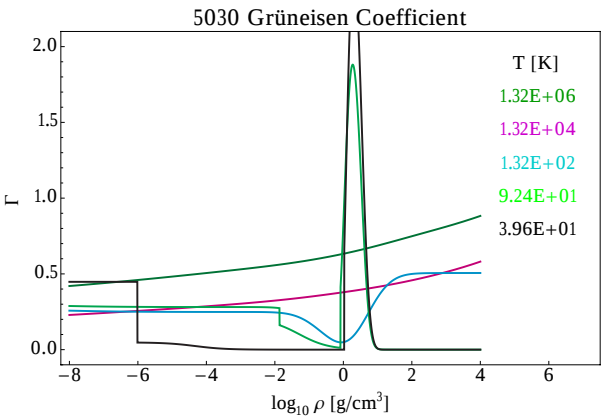
5030 Grüneisen Coefficient
Γ
log10 ρ [g/cm3]
T [K]
1.32E+06
1.32E+04
1.32E+02
9.24E+01
3.96E+01

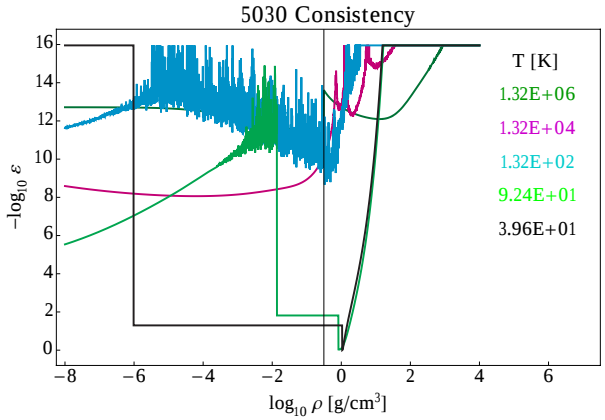
5030 Consistency
−log10 ε
log10 ρ [g/cm3]
T [K]
1.32E+06
1.32E+04
1.32E+02
9.24E+01
3.96E+01

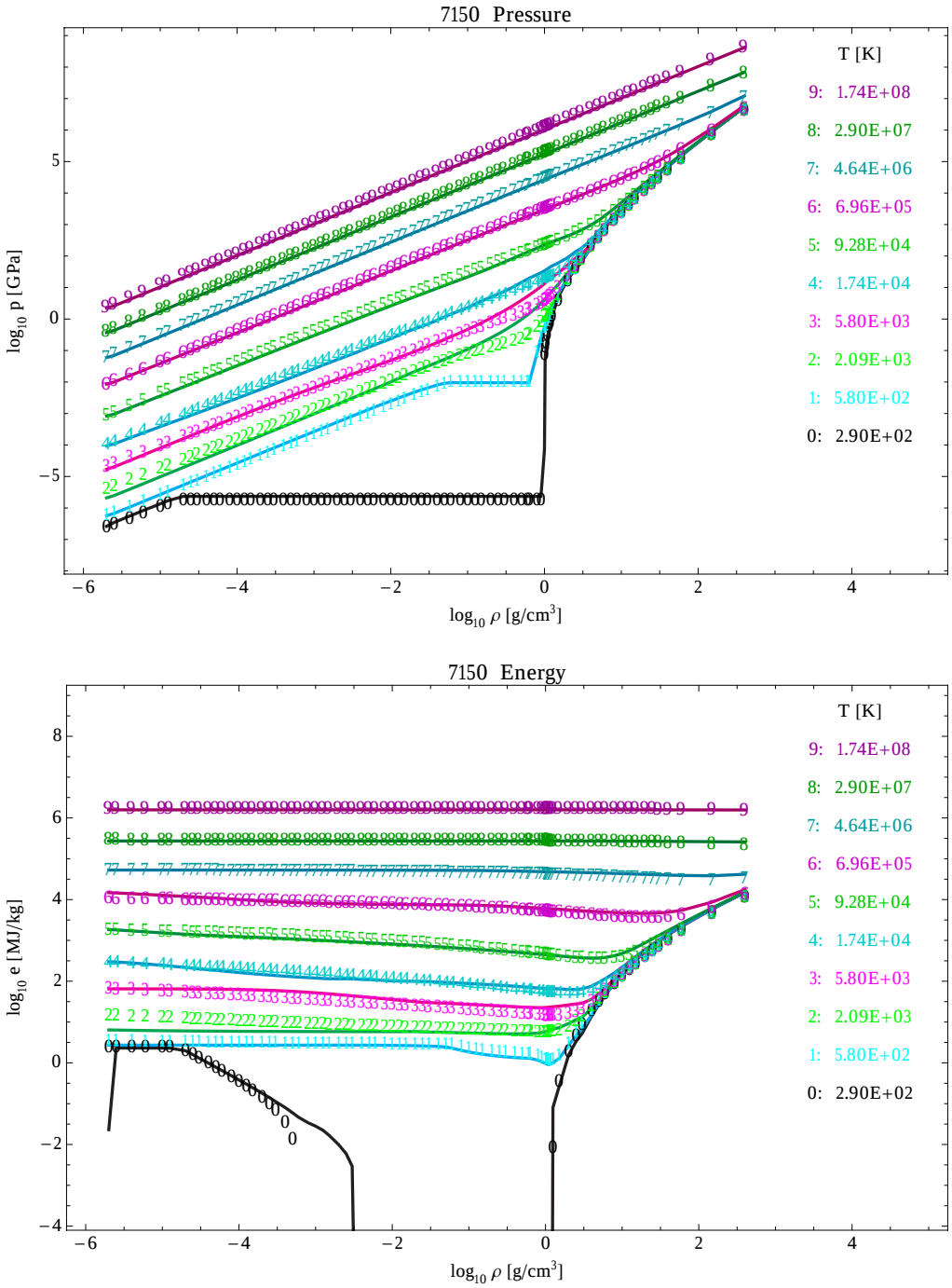

Comparison of the MGGB fit to Sesame 7150 Water. Top $p\,[v,T]$; bottom $e\,[v,T]$; solid line connects the Sesame tabular data points; symbols mark the MGGB fit evaluated at the Sesame $[v,T]$ points.

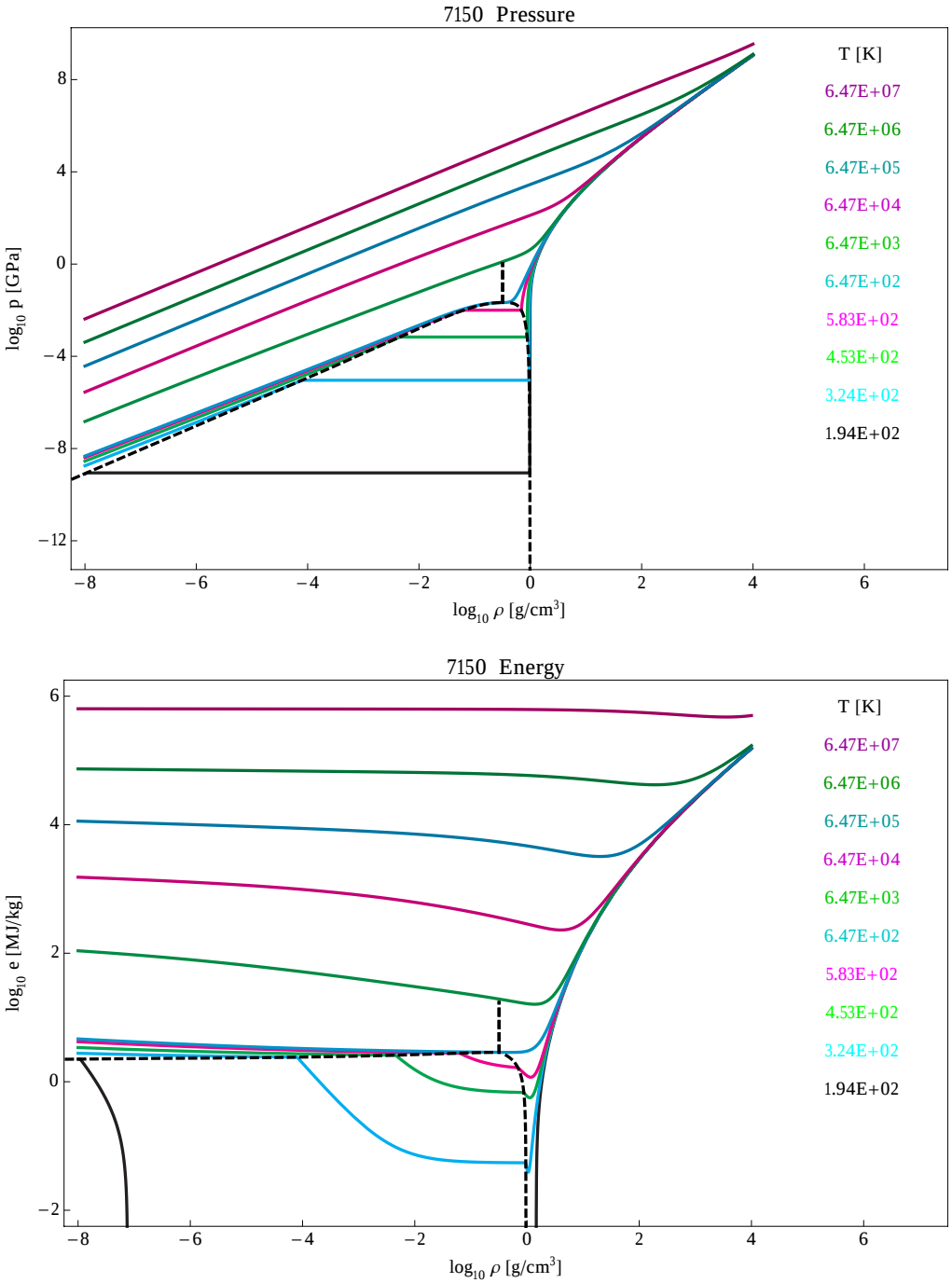

MGGB 5030 Water.

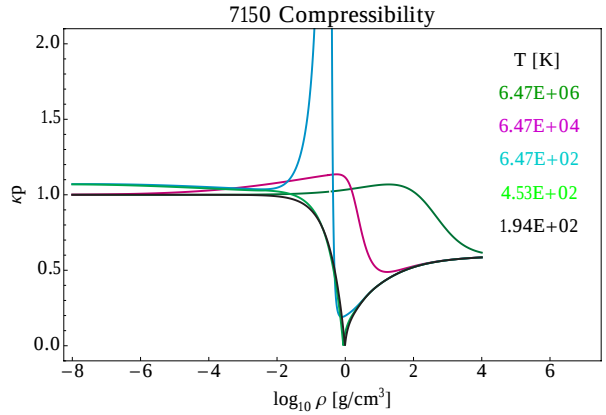
7150 Compressibility
κp
log10 ρ [g/cm3]
T [K]
6.47E+06
6.47E+04
6.47E+02
4.53E+02
1.94E+02

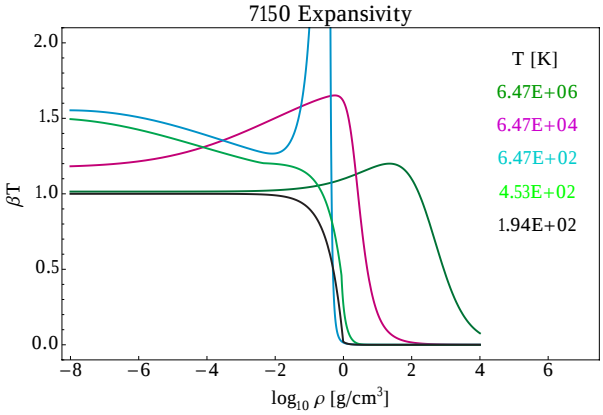
7150 Expansivity
βT
log10 ρ [g/cm3]
T [K]
6.47E+06
6.47E+04
6.47E+02
4.53E+02
1.94E+02

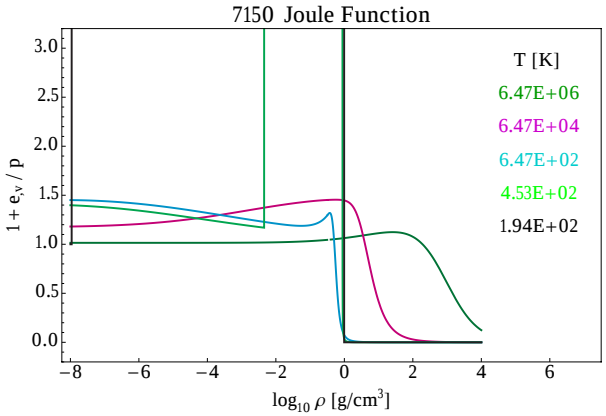
7150 Joule Function
1 + ev / p
log10 ρ [g/cm3]
T [K]
6.47E+06
6.47E+04
6.47E+02
4.53E+02
1.94E+02

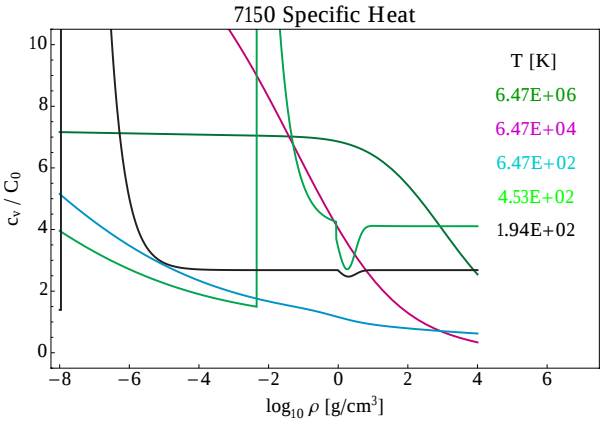
7150 Specific Heat
cv / C0
log10 ρ [g/cm3]
T [K]
6.47E+06
6.47E+04
6.47E+02
4.53E+02
1.94E+02

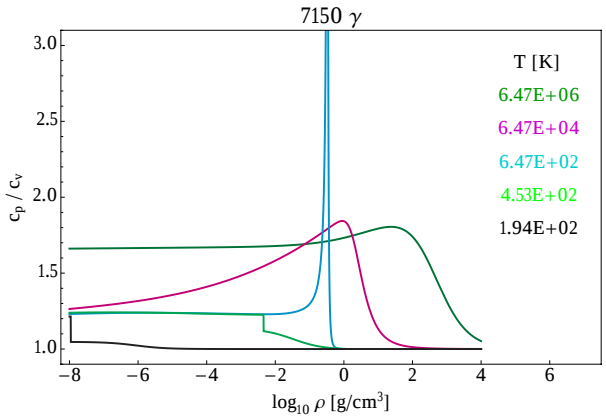
7150 γ
cp / cv
log10 ρ [g/cm3]
T [K]
6.47E+06
6.47E+04
6.47E+02
4.53E+02
1.94E+02

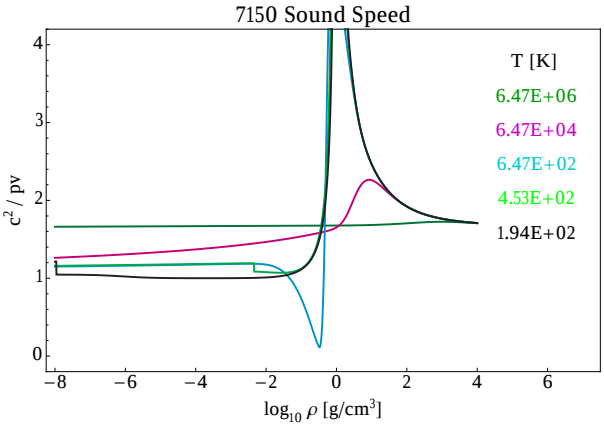
7150 Sound Speed
c2 / pv
log10 ρ [g/cm3]
T [K]
6.47E+06
6.47E+04
6.47E+02
4.53E+02
1.94E+02

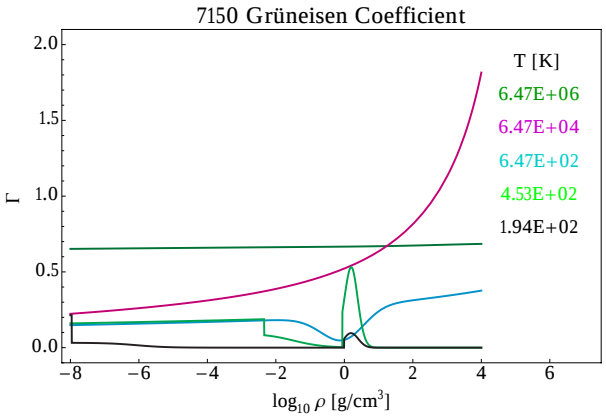
7150 Grüneisen Coefficient
Γ
log10 ρ [g/cm3]
T [K]
6.47E+06
6.47E+04
6.47E+02
4.53E+02
1.94E+02

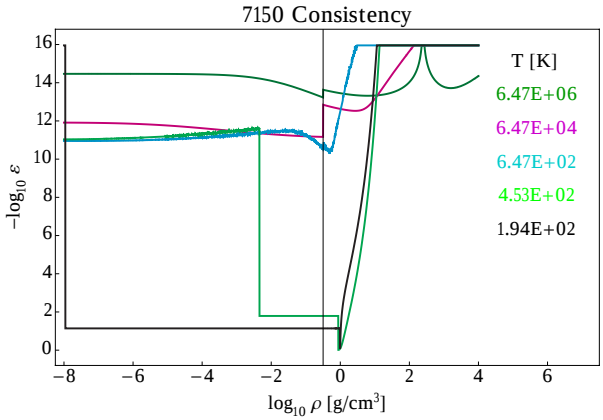
7150 Consistency
−log10 ε
log10 ρ [g/cm3]
T [K]
6.47E+06
6.47E+04
6.47E+02
4.53E+02
1.94E+02

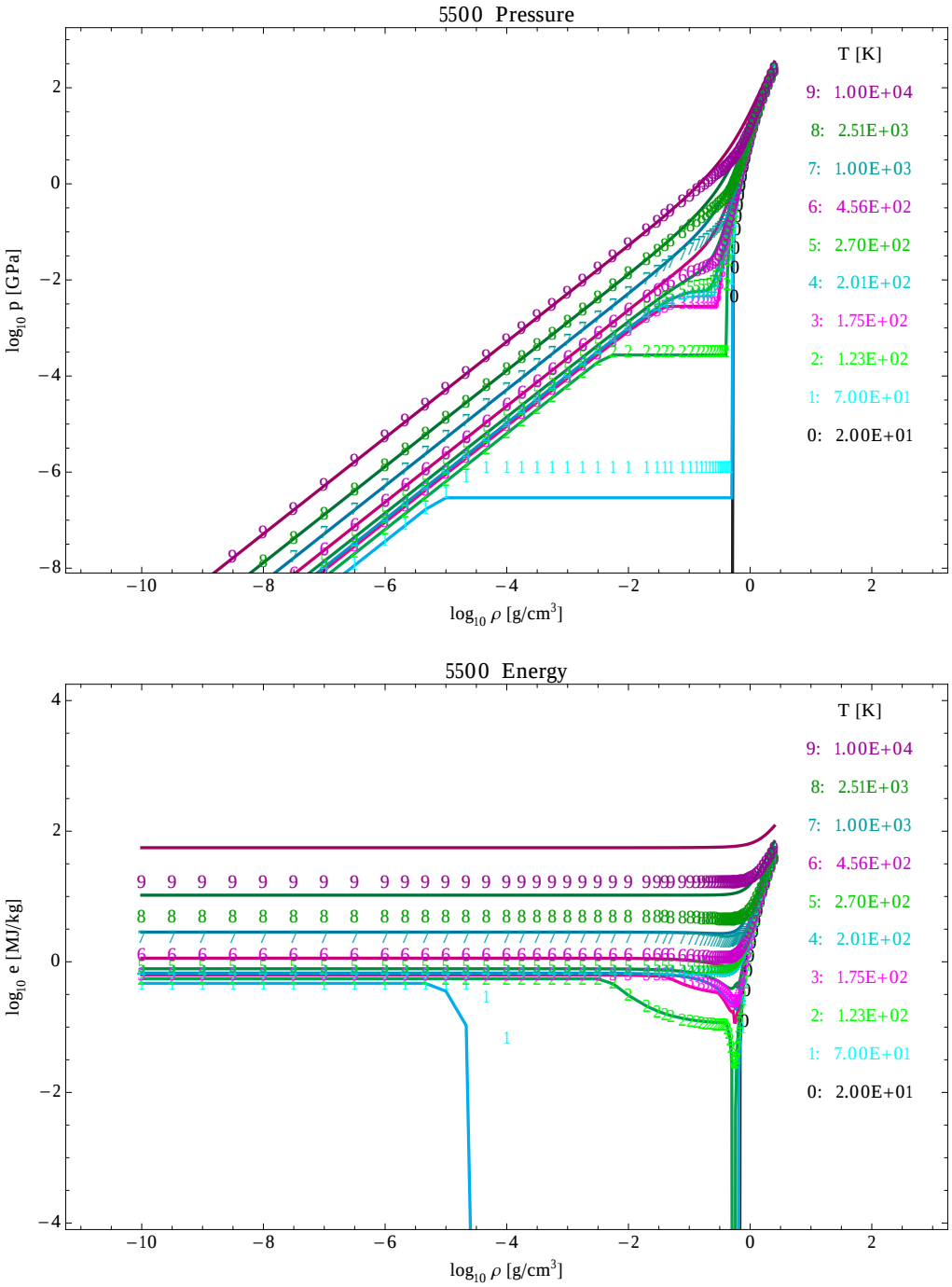

Comparison of the MGGB fit to Sesame 5500 Methane. Top $p\,[v,T]$; bottom $e\,[v,T]$; solid line connects the Sesame tabular data points; symbols mark the MGGB fit evaluated at the Sesame $[v,T]$ points.

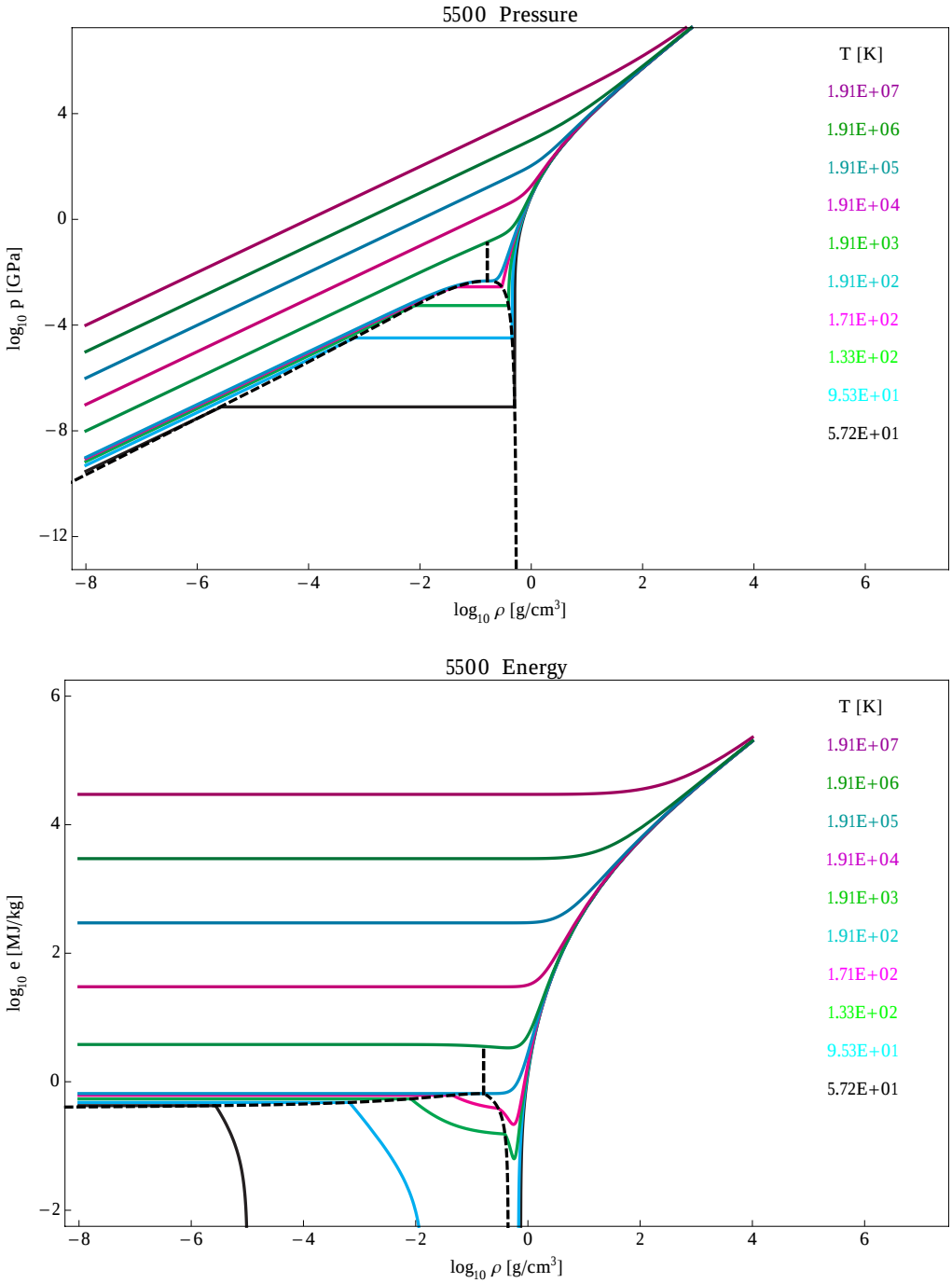

MGGB 5500 Methane.

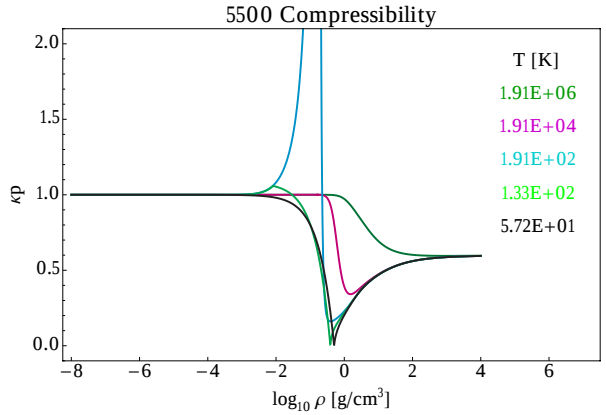
5500 Compressibility
κp
log10 ρ [g/cm3]
T [K]
1.91E+06
1.91E+04
1.91E+02
1.33E+02
5.72E+01

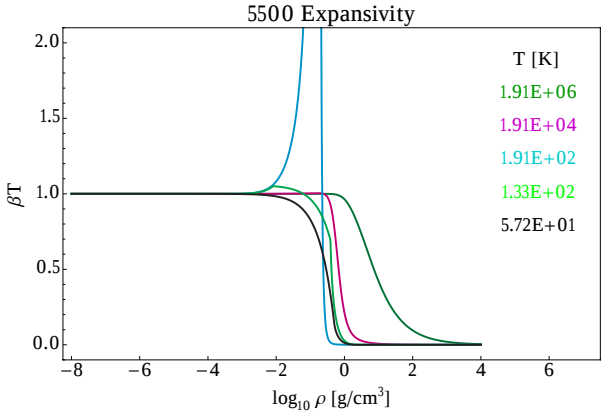
5500 Expansivity
βT
log10 ρ [g/cm3]
T [K]
1.91E+06
1.91E+04
1.91E+02
1.33E+02
5.72E+01

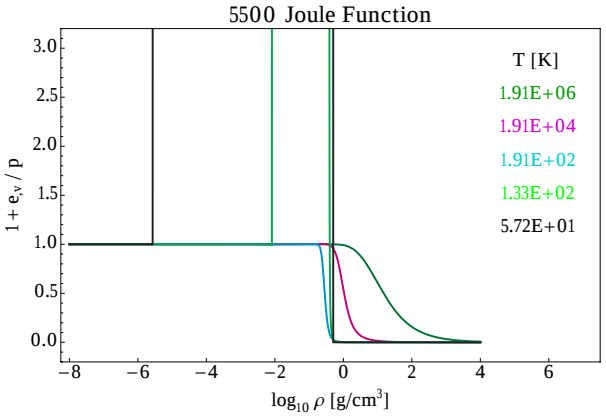
5500 Joule Function
1 + ev / p
log10 ρ [g/cm3]
T [K]
1.91E+06
1.91E+04
1.91E+02
1.33E+02
5.72E+01

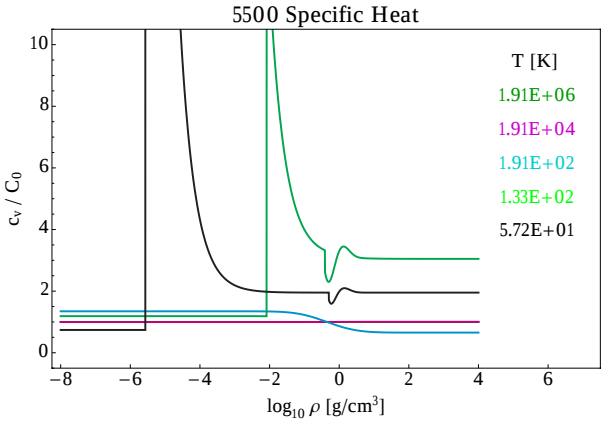
5500 Specific Heat
cv / C0
log10 ρ [g/cm3]
T [K]
1.91E+06
1.91E+04
1.91E+02
1.33E+02
5.72E+01

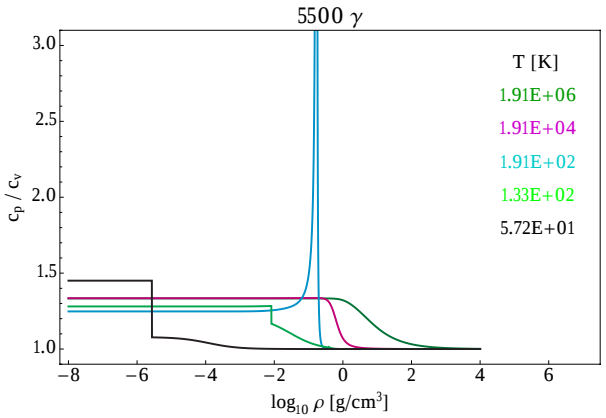
5500 γ
cp / cv
log10 ρ [g/cm3]
T [K]
1.91E+06
1.91E+04
1.91E+02
1.33E+02
5.72E+01

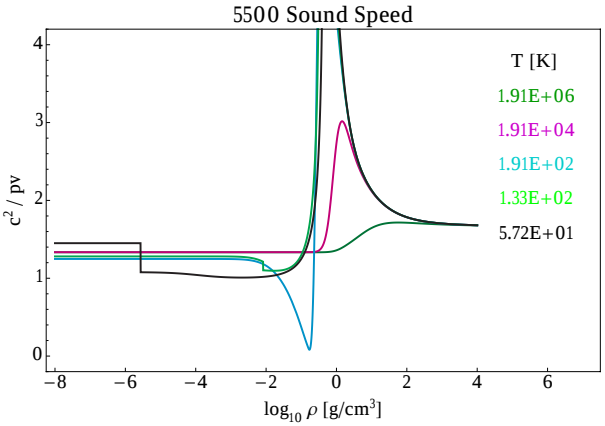
5500 Sound Speed
c2 / pv
log10 ρ [g/cm3]
T [K]
1.91E+06
1.91E+04
1.91E+02
1.33E+02
5.72E+01

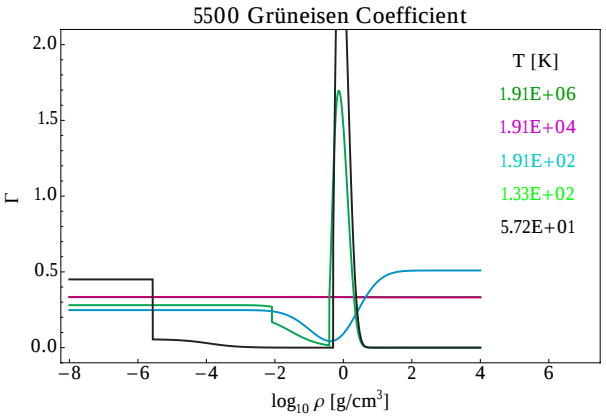
5500 Grüneisen Coefficient
Γ
log10 ρ [g/cm3]
T [K]
1.91E+06
1.91E+04
1.91E+02
1.33E+02
5.72E+01

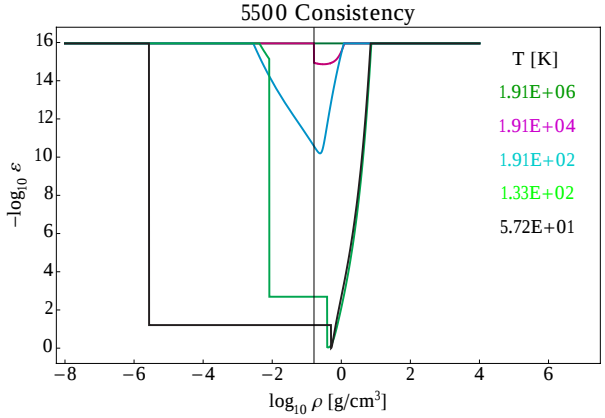
5500 Consistency
−log10 ε
log10 ρ [g/cm3]
T [K]
1.91E+06
1.91E+04
1.91E+02
1.33E+02
5.72E+01

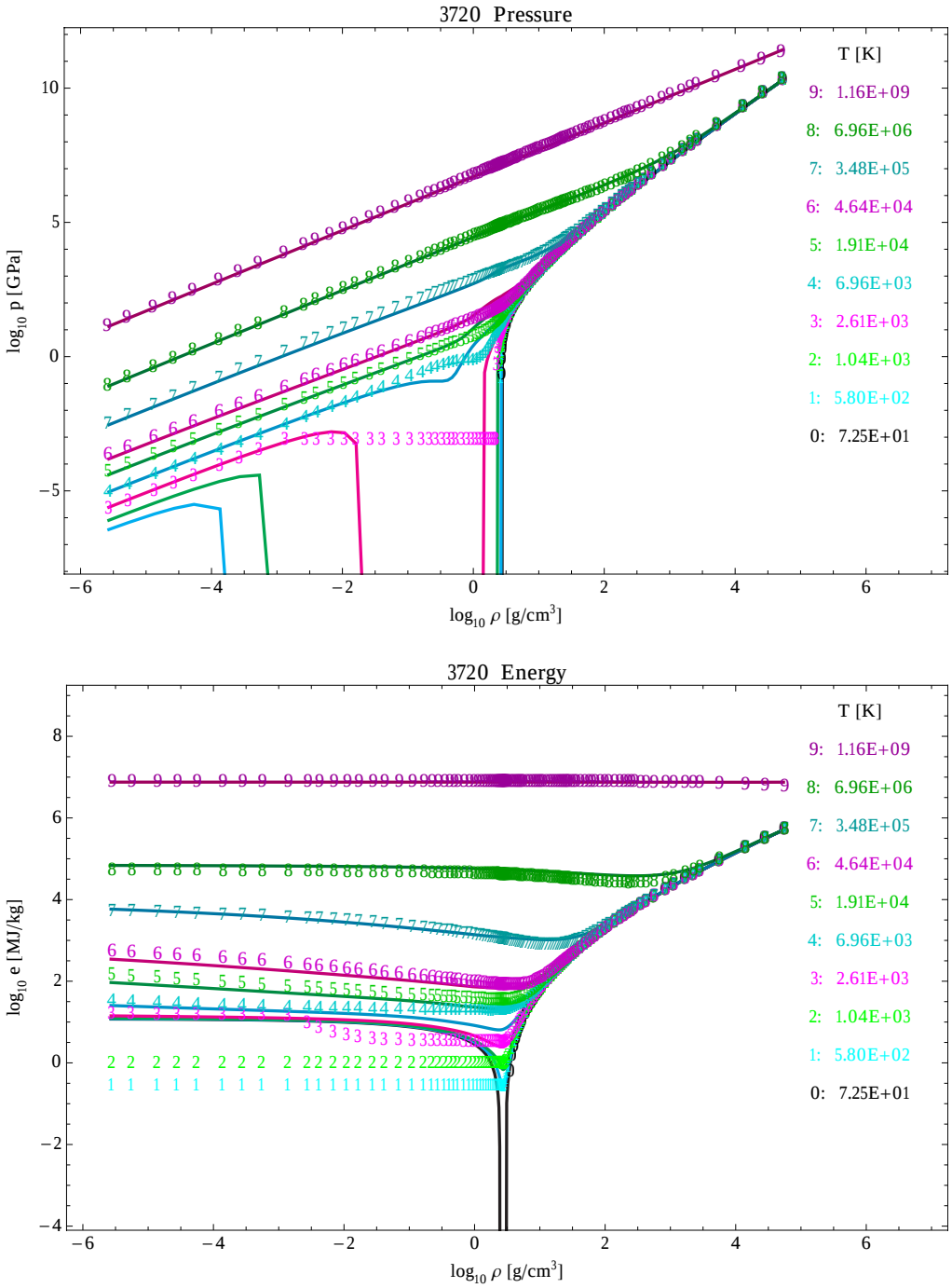

Comparison of the MGGB fit to Sesame 3720 Aluminum. Top $p\,[v,T]$; bottom $e\,[v,T]$; solid line connects the Sesame tabular data points; symbols mark the MGGB fit evaluated at the Sesame $[v,T]$ points.

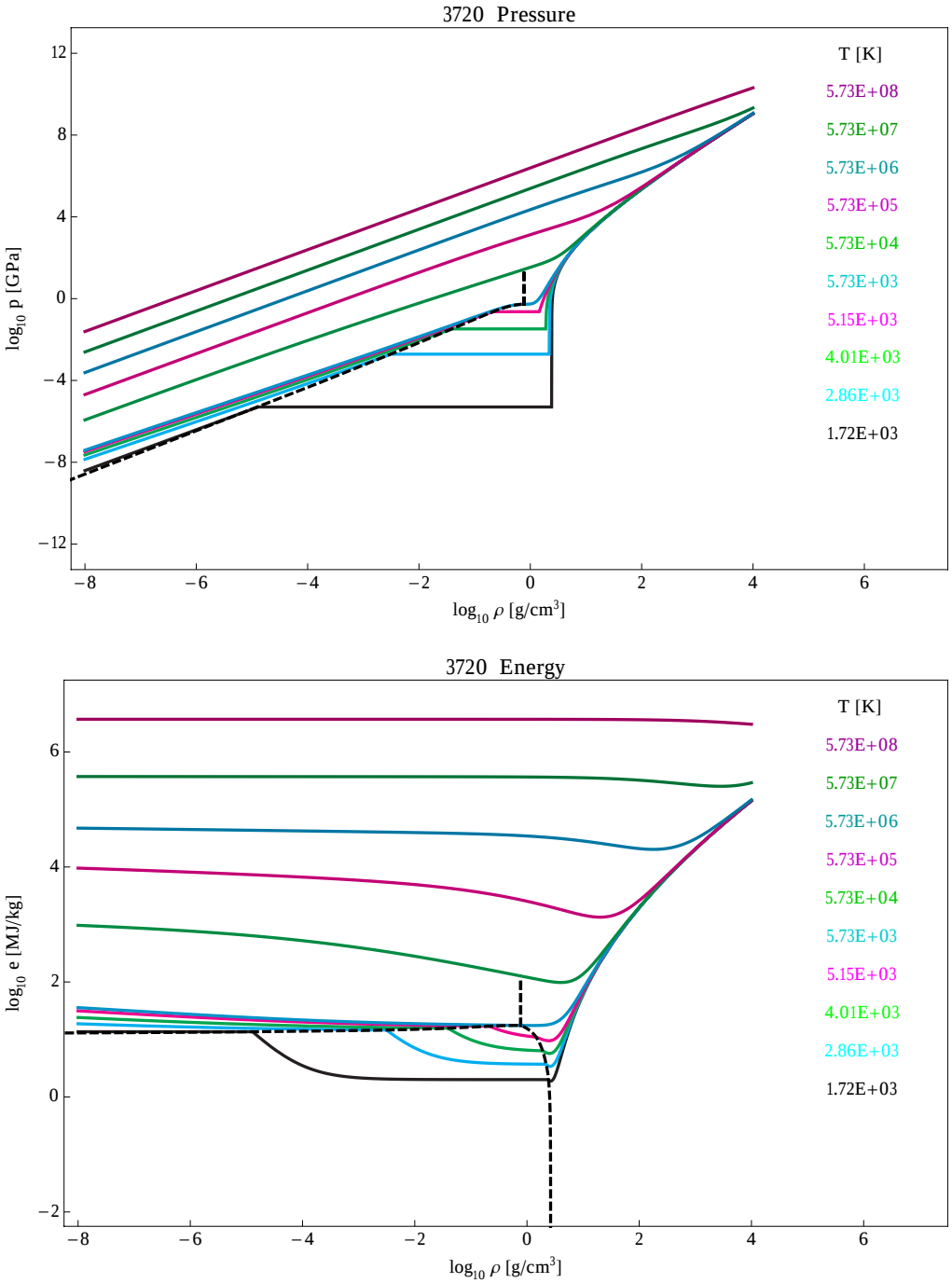

MGGB 3720 Aluminum.

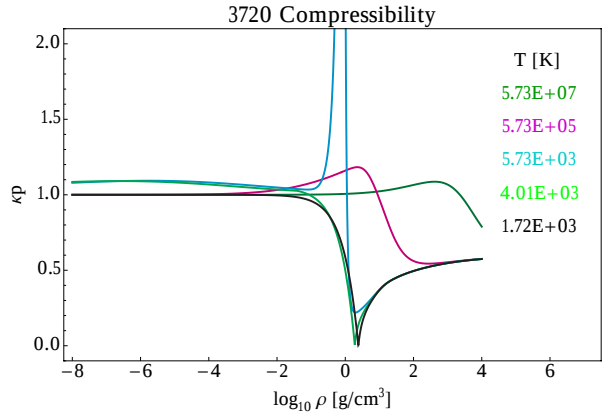
3720 Compressibility
κp
log10 ρ [g/cm3]
T [K]
5.73E+07
5.73E+05
5.73E+03
4.01E+03
1.72E+03

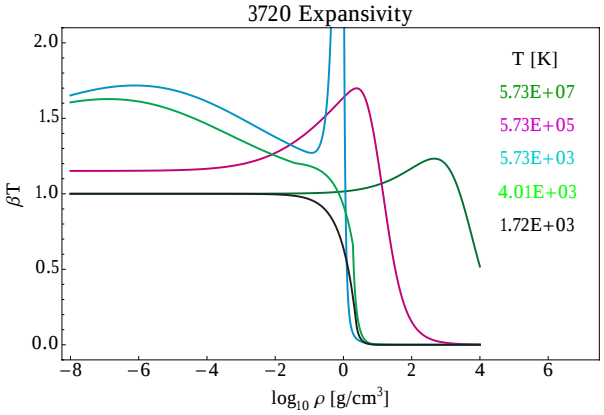
3720 Expansivity
βT
log10 ρ [g/cm3]
T [K]
5.73E+07
5.73E+05
5.73E+03
4.01E+03
1.72E+03

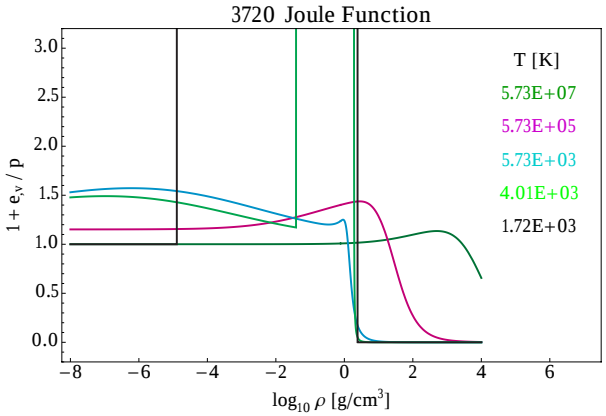
3720 Joule Function
1 + ev / p
log10 ρ [g/cm3]
T [K]
5.73E+07
5.73E+05
5.73E+03
4.01E+03
1.72E+03

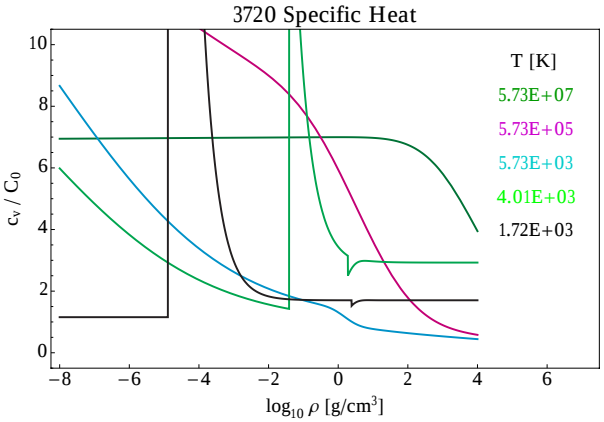
3720 Specific Heat
cv / C0
log10 ρ [g/cm3]
T [K]
5.73E+07
5.73E+05
5.73E+03
4.01E+03
1.72E+03

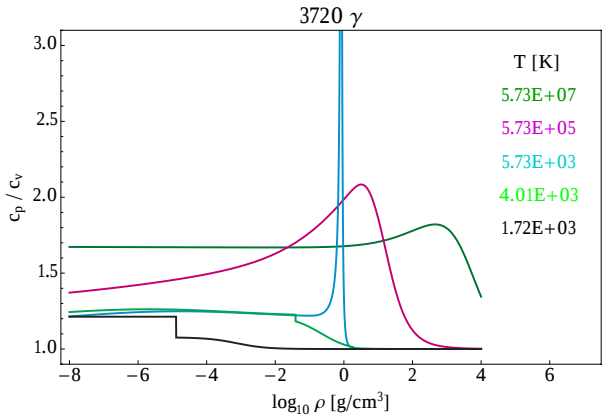
3720 γ
cp / cv
log10 ρ [g/cm3]
T [K]
5.73E+07
5.73E+05
5.73E+03
4.01E+03
1.72E+03

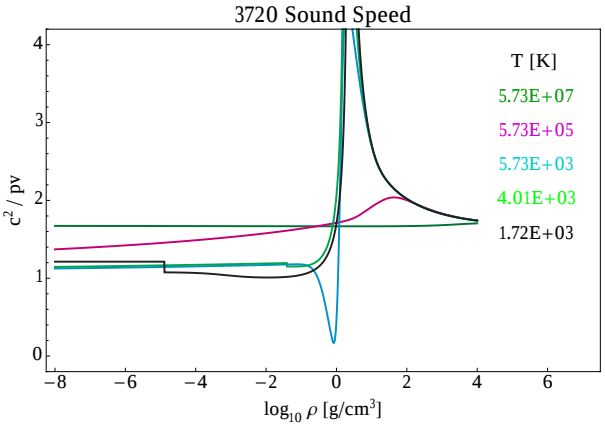
3720 Sound Speed
c2 / pv
log10 ρ [g/cm3]
T [K]
5.73E+07
5.73E+05
5.73E+03
4.01E+03
1.72E+03

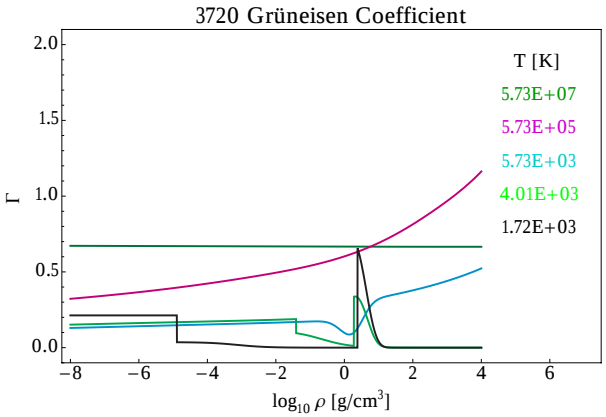
3720 Grüneisen Coefficient
Γ
log10 ρ [g/cm3]
T [K]
5.73E+07
5.73E+05
5.73E+03
4.01E+03
1.72E+03

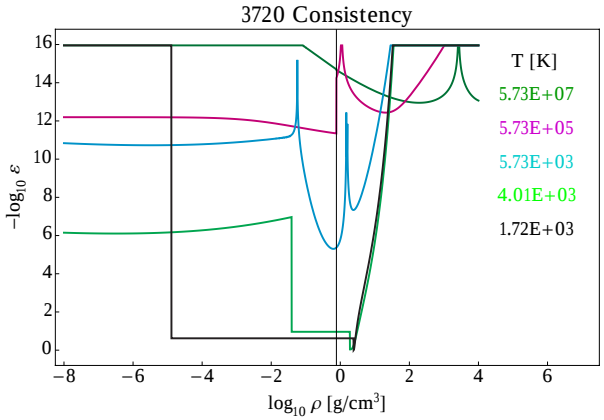
3720 Consistency
−log10 ε
log10 ρ [g/cm3]
T [K]
5.73E+07
5.73E+05
5.73E+03
4.01E+03
1.72E+03

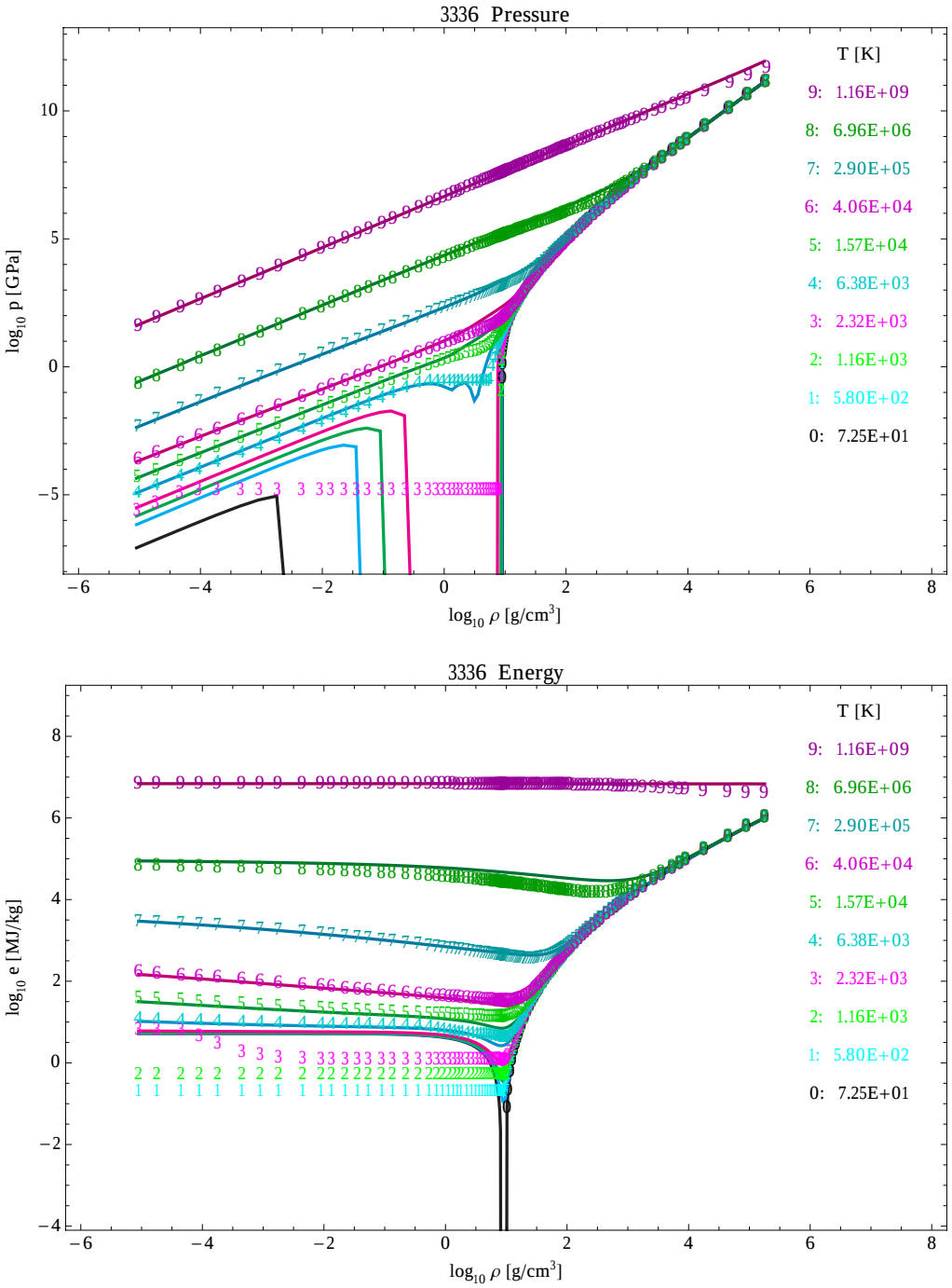

Comparison of the MGGB fit to Sesame 3336 Copper. Top $p\,[v,T]$; bottom $e\,[v,T]$; solid line connects the Sesame tabular data points; symbols mark the MGGB fit evaluated at the Sesame $[v,T]$ points.

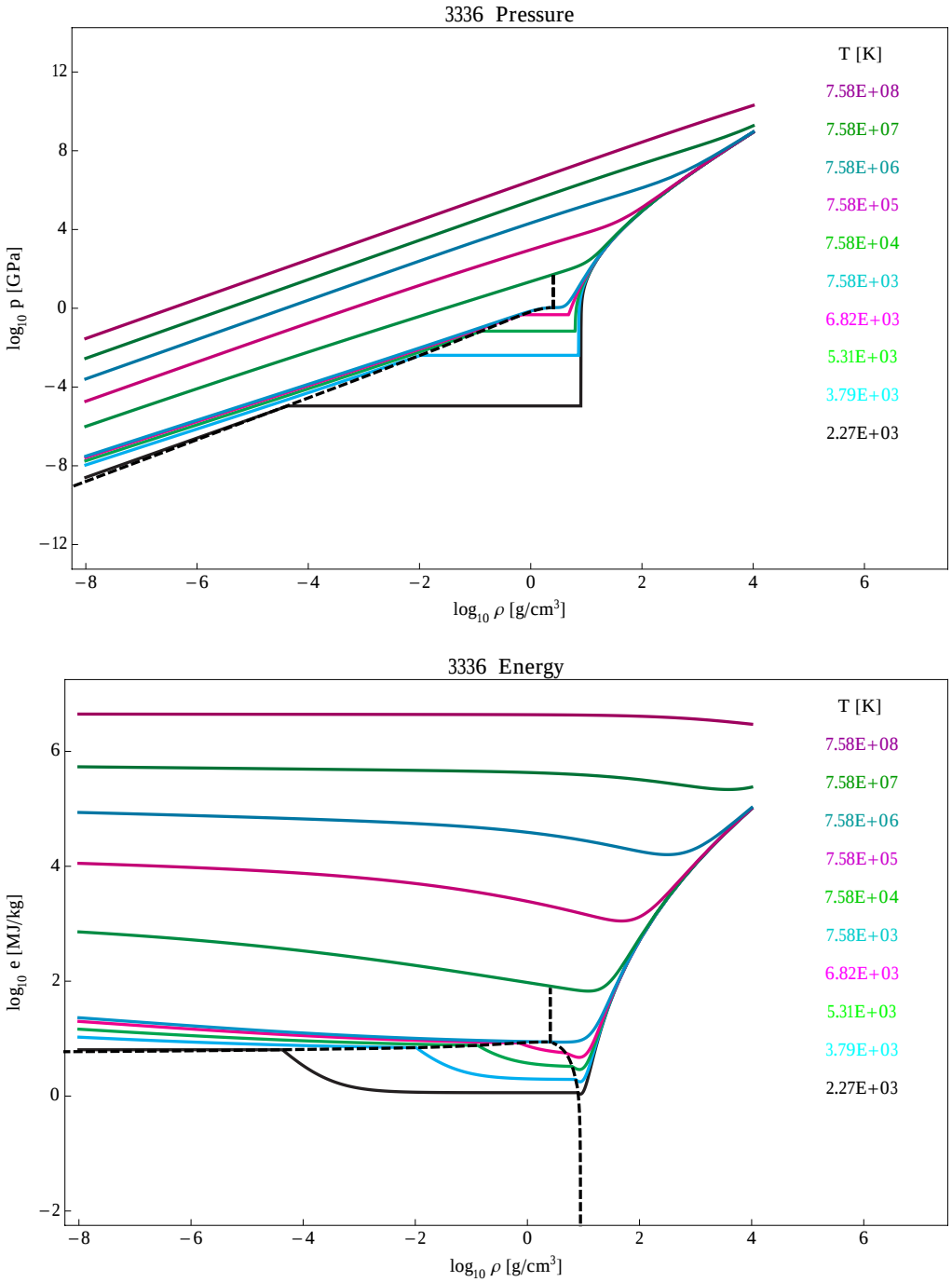

MGGB 3336 Copper.

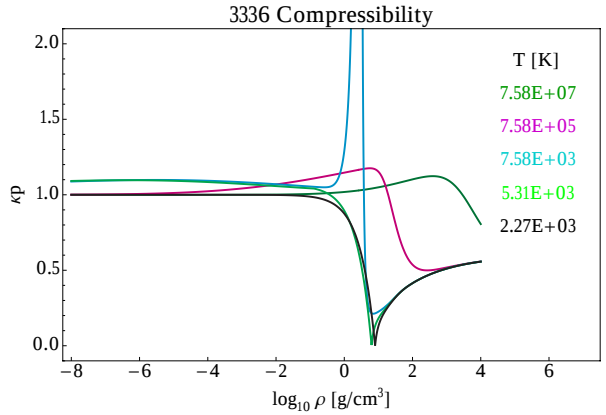
3336 Compressibility
κp
log10 ρ [g/cm3]
T [K]
7.58E+07
7.58E+05
7.58E+03
5.31E+03
2.27E+03

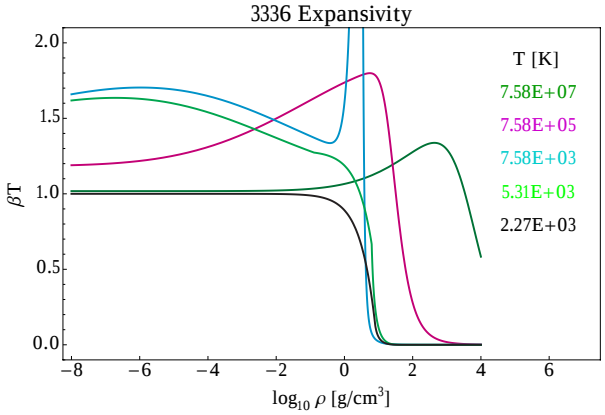
3336 Expansivity
βT
log10 ρ [g/cm3]
T [K]
7.58E+07
7.58E+05
7.58E+03
5.31E+03
2.27E+03

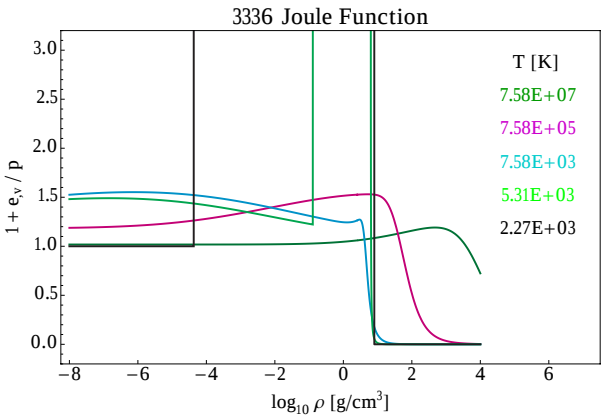
3336 Joule Function
1 + ev / p
log10 ρ [g/cm3]
T [K]
7.58E+07
7.58E+05
7.58E+03
5.31E+03
2.27E+03

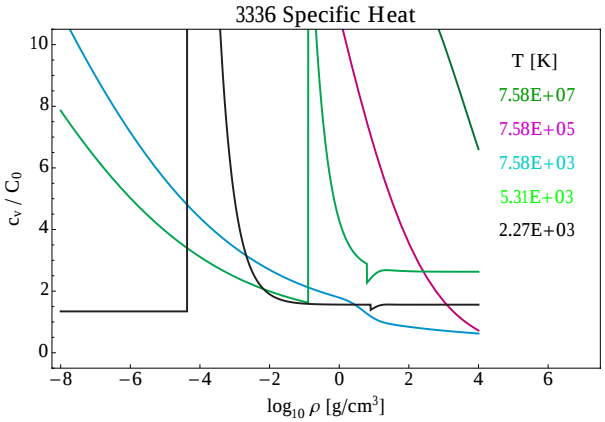
3336 Specific Heat
cv / C0
log10 ρ [g/cm3]
T [K]
7.58E+07
7.58E+05
7.58E+03
5.31E+03
2.27E+03

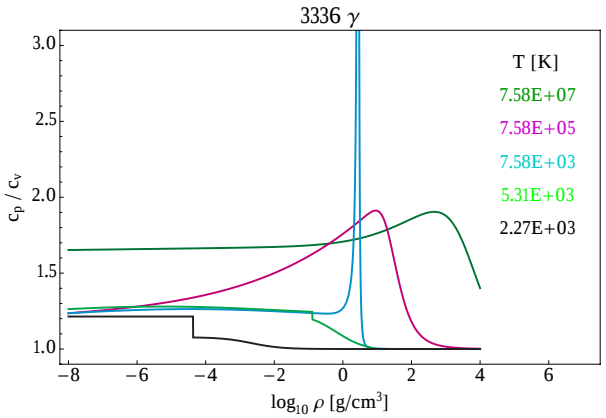
3336 γ
cp / cv
log10 ρ [g/cm3]
T [K]
7.58E+07
7.58E+05
7.58E+03
5.31E+03
2.27E+03

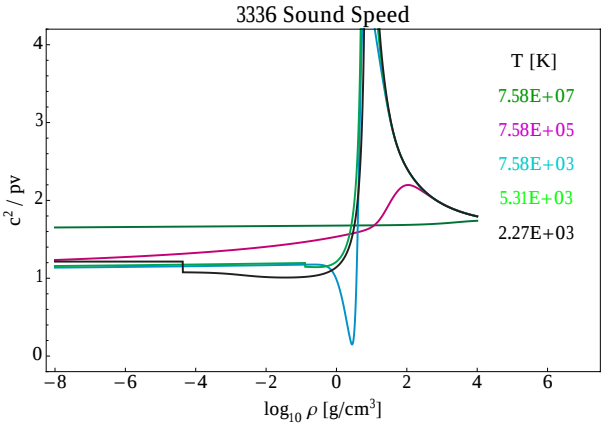
3336 Sound Speed
c2 / pv
log10 ρ [g/cm3]
T [K]
7.58E+07
7.58E+05
7.58E+03
5.31E+03
2.27E+03

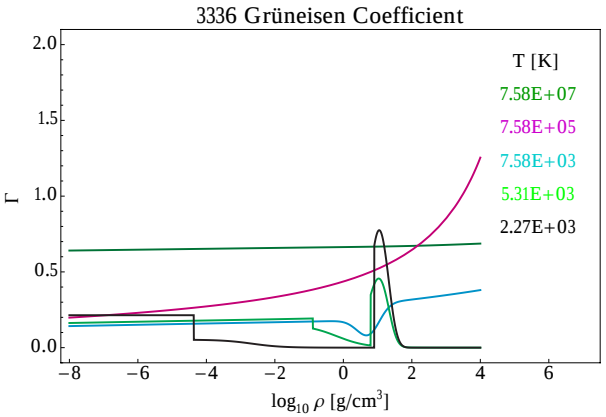
3336 Grüneisen Coefficient
Γ
log10 ρ [g/cm3]
T [K]
7.58E+07
7.58E+05
7.58E+03
5.31E+03
2.27E+03

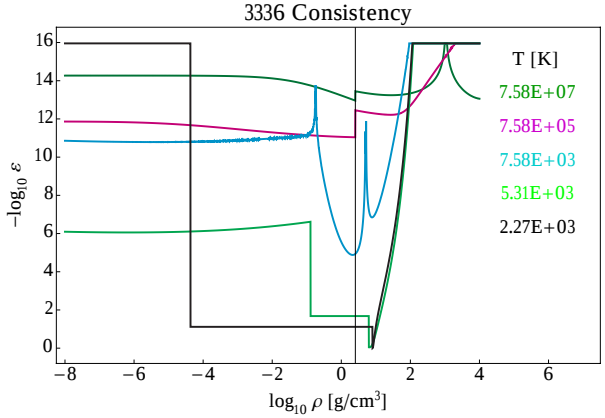
3336 Consistency
−log10 ε
log10 ρ [g/cm3]
T [K]
7.58E+07
7.58E+05
7.58E+03
5.31E+03
2.27E+03

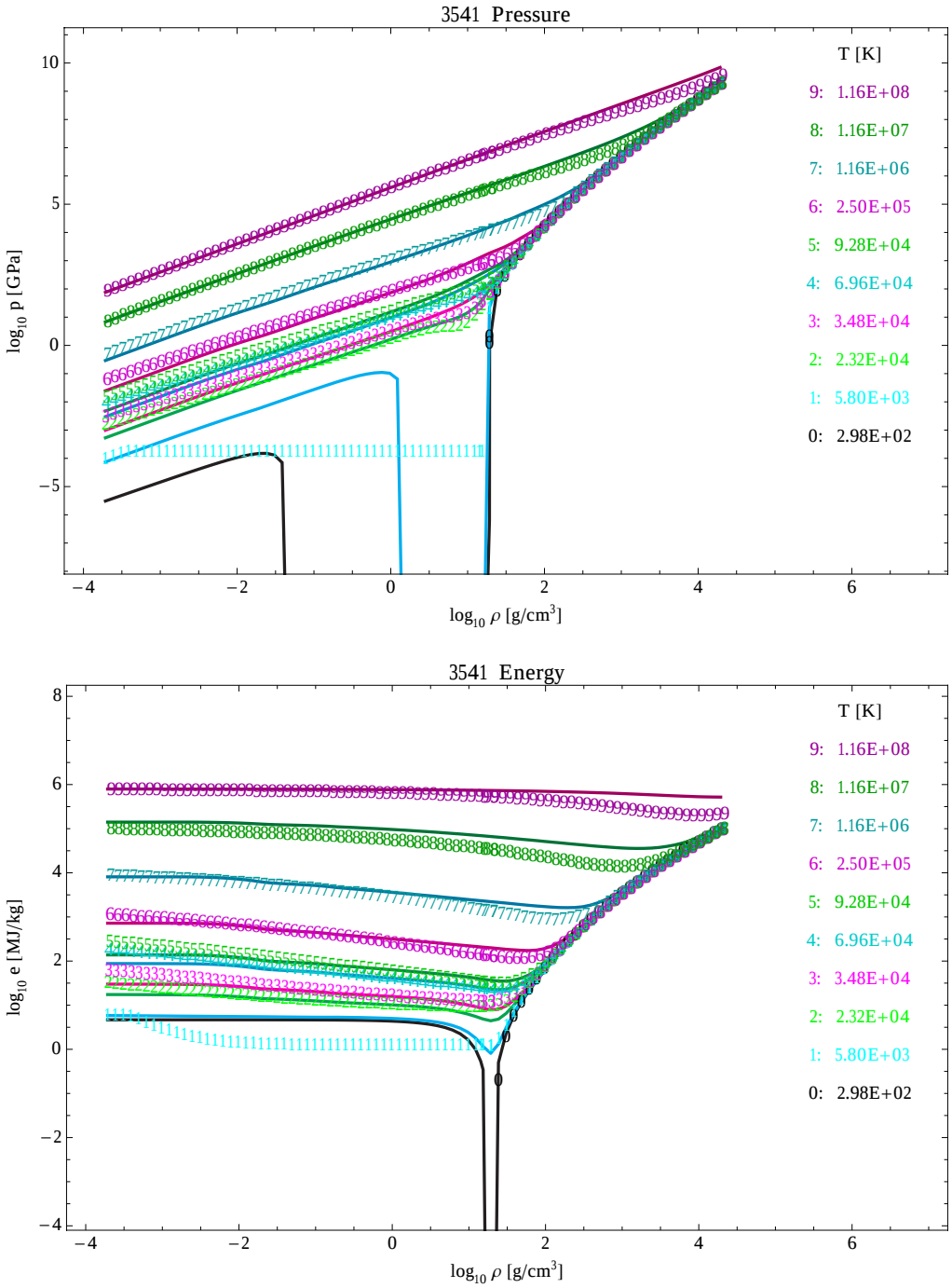

Comparison of the MGGB fit to Sesame 3541 Tungsten. Top $p\,[v,T]$; bottom $e\,[v,T]$; solid line connects the Sesame tabular data points; symbols mark the MGGB fit evaluated at the Sesame $[v,T]$ points.

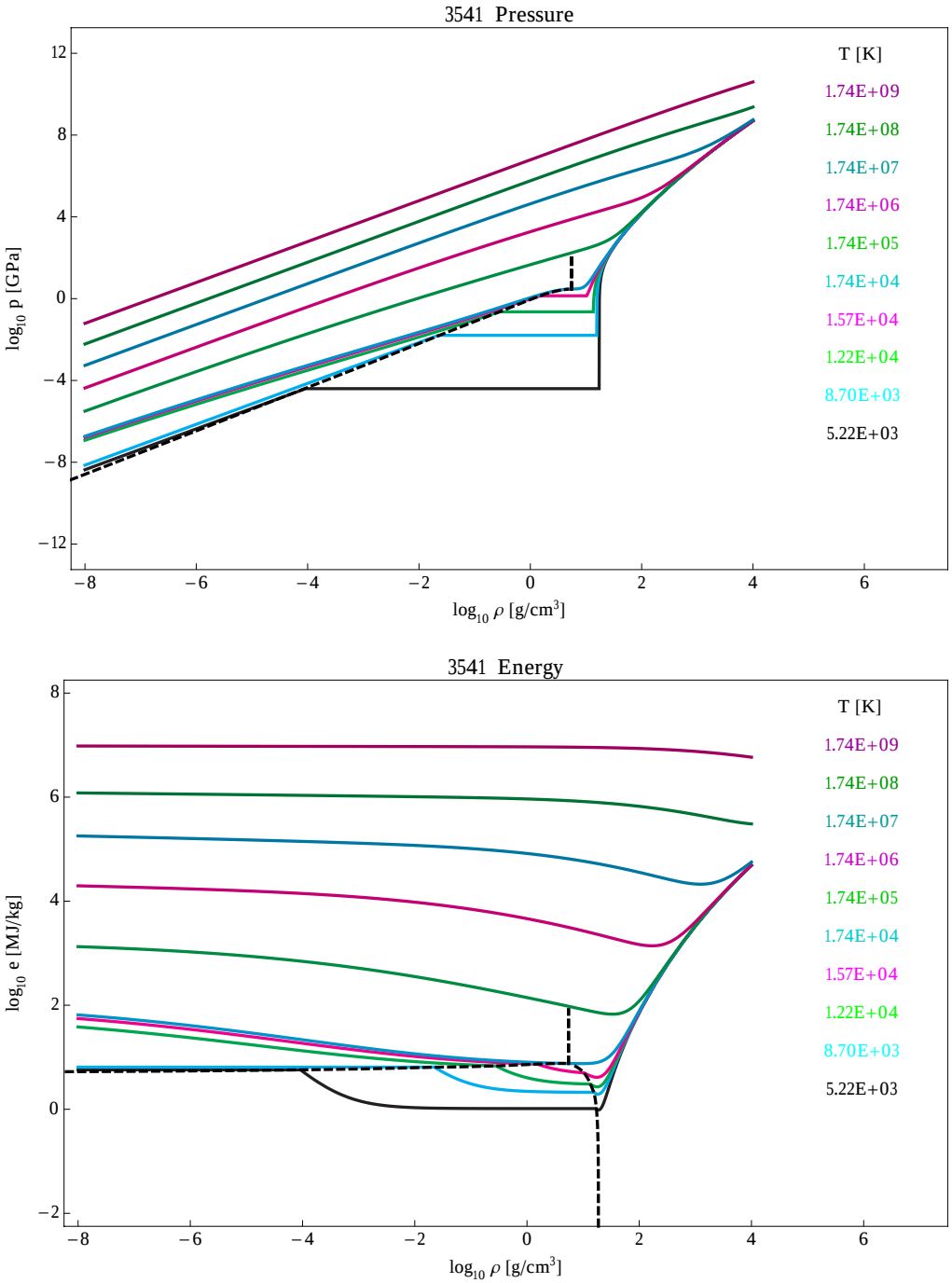

MGGB 3541 Tungsten.

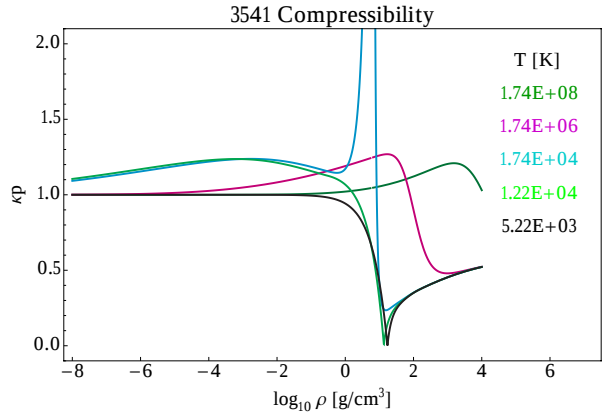
3541 Compressibility
κp
log10 ρ [g/cm3]
T [K]
1.74E+08
1.74E+06
1.74E+04
1.22E+04
5.22E+03

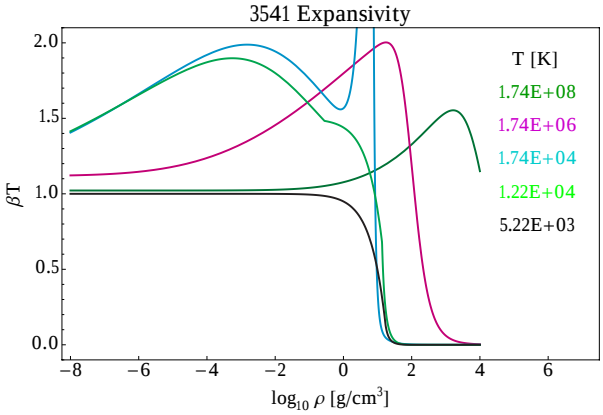
3541 Expansivity
βT
log10 ρ [g/cm3]
T [K]
1.74E+08
1.74E+06
1.74E+04
1.22E+04
5.22E+03

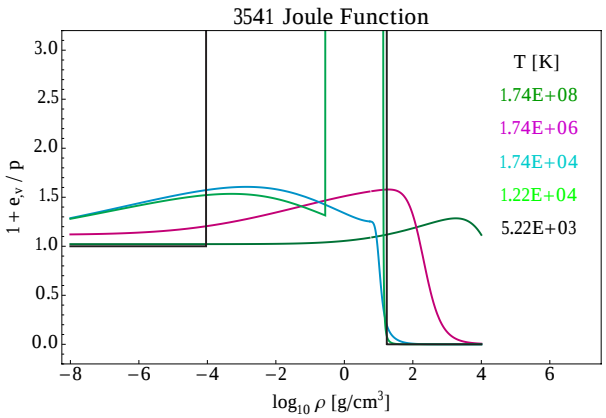
3541 Joule Function
1 + ev / p
log10 ρ [g/cm3]
T [K]
1.74E+08
1.74E+06
1.74E+04
1.22E+04
5.22E+03

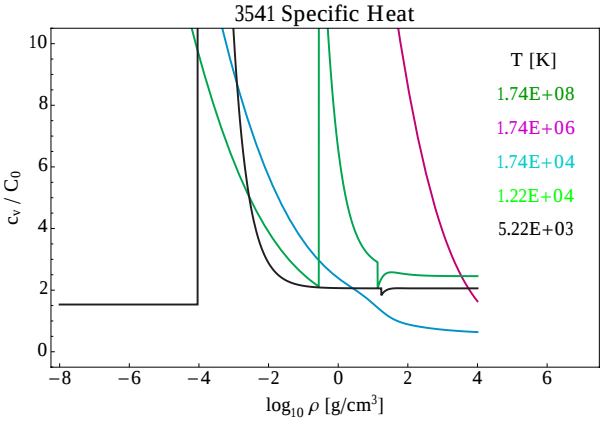
3541 Specific Heat
cv / C0
log10 ρ [g/cm3]
T [K]
1.74E+08
1.74E+06
1.74E+04
1.22E+04
5.22E+03

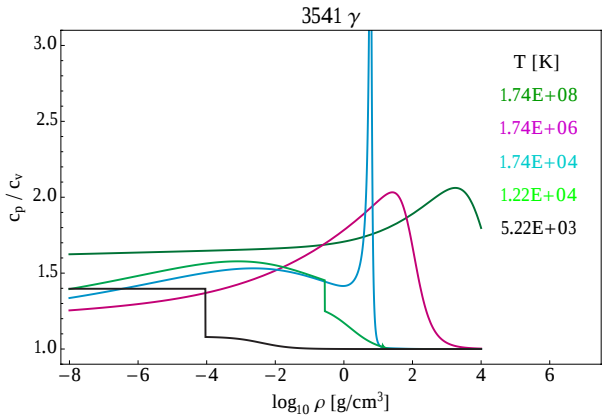
3541 γ
cp / cv
log10 ρ [g/cm3]
T [K]
1.74E+08
1.74E+06
1.74E+04
1.22E+04
5.22E+03

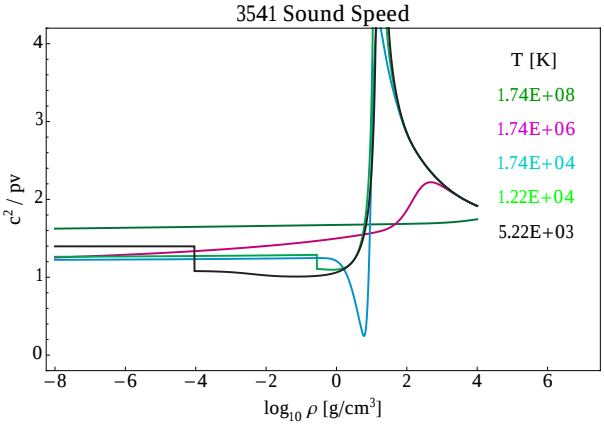
3541 Sound Speed
c2 / pv
log10 ρ [g/cm3]
T [K]
1.74E+08
1.74E+06
1.74E+04
1.22E+04
5.22E+03

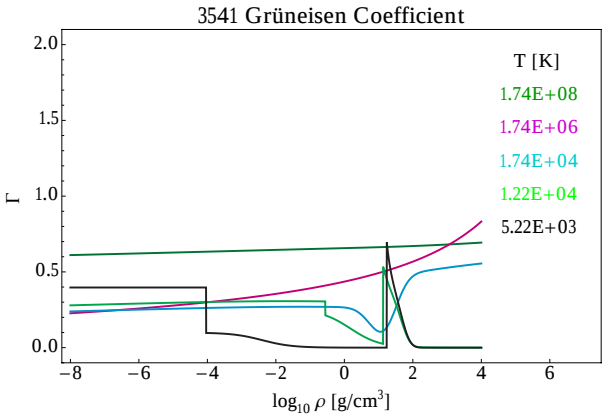
3541 Grüneisen Coefficient
Γ
log10 ρ [g/cm3]
T [K]
1.74E+08
1.74E+06
1.74E+04
1.22E+04
5.22E+03

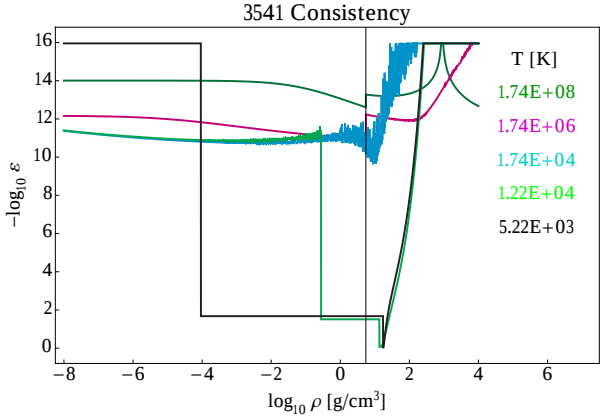
3541 Consistency
−log10 ε
log10 ρ [g/cm3]
T [K]
1.74E+08
1.74E+06
1.74E+04
1.22E+04
5.22E+03


Los Alamos
NATIONAL LABORATORY
EST. 1943